Author's response

We would like to thank the referees for their comments. We attach the responses to both referees (blue) with their original comments (black). Below this, we attach the latest tracked version of the manuscript.

Responses to Referee 1 (R1)

The manuscript of Sanchez-Marroquin et al. deals with the characterization of an aircraft inlet frequently used in the British BAE-146 research aircraft. Despite of the importance of inlet characterization, it happens frequently that aerosol inlets are built and used, but remain uncharacterized. Therefore, these type of studies is valuable to rate the results of aerosol research done with the according systems, in particular with respect to their (size) representativity.

The authors compare an experimental approach for inlet transmission characterization with a theory-based one and come to the conclusion of a general approximate agreement. They propose a range of operational conditions based on their results.

The paper is mostly well-written; the methods are explained and applied. Some unclear sections remain (detailed below). References are adequate. However, some effort should be placed into the thermodynamic considerations, and the SEM part should be structured partly into a second publication. Also, some intentions for future work are given scattered through the paper, which should be either moved to the motivation section or omitted.

Thank you very much for this comments. They are very useful and will definitely improve the manuscript. We address the specific comments below.

General remarks
The paper goes into details about aerosol flows, but the properties and values reported in the text should be treated with more precision. E.g., flow rates are reported in L per minute, but it is unclear, whether this means volumetric L at the outside conditions, volumetric L at the inlet conditions, mass equivalent L at standard conditions.
Line Added in Sect. 2.1: "The air flow through the filter (filter flow) is measured by a mass flow meter, which measures the sampled air mass and reports it in equivalent litres at standard conditions (273.15 k, 1013.529 hPa)".
Line Added in Sect. 2.2: (volumetric L at standard conditions: 273.15 k, 1013.529 hPa),
Line Added in Sect. 2.2: (all the flow rates of our calculations are given in L min-1 at standard conditions: 273.15 k, 1013.529 hPa).

636-637: "All calculation were done under standard conditions" – Why? Most aerosol/carrier gas interactions depend on the air viscosity and free mean path, some on Reynolds number and therefore density. As result, most efficiency functions at the end have temperature and density in them. It doesn't seem to be a wise choice to neglect these dependencies, in particular not for aircraft measurements with their strong variation. Also, the thermodynamic conditions change considerably from the outside conditions through in inlet and tubing to the filter. Estimates were done using 'classical' aerosol aspiration / transmission formulas, which don't appear to be relevant in all cases (see detailed comments). A major question in this context is why the authors decided not to use computational fluid dynamics modelling. While these techniques are work-intensive and in turbulent situations also not necessarily precise, in particular for the inlet, diffusor and bend / inertial separator section, they might have been more useful.
C2
A temperature and pressure dependence test was performed. In the figure below, one can see the total efficiency for the 40L/min case (including the diffusion) for standard conditions, International standard atmosphere conditions at 0 and 3000m (the range in which the filter inlet system works. The differences are negligible. A similar negligible dependence was calculated for another inlet on board of the FAAM aircraft in Trembath (2012).

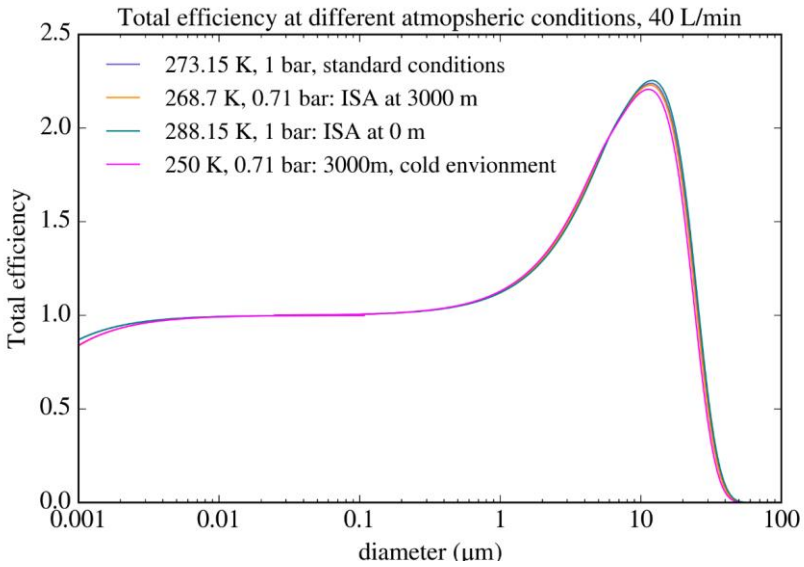

Line added at the third paragraph of Appendix A: "The effect of changes in pressure and temperature (and therefore air density and dynamic viscosity) that normally occur in the filter inlet system sampling range (0 to 3000 m) are negligible in all the used equations".

Further thermodynamic analysis in order to estimate the heating losses are impossible to carry out because of the lack of temperature and pressure measurement instruments through the inlet, which are not possible to have because of certification issues. This is a frequent problem of aircraft research. This is now mentioned in section:

Added in fourth paragraph of Sect. 5: "Also, volatilization of certain type of aerosol particles (which are more abundant in the submicron fraction (Seinfeld and Pandis, 2006)) can happen during heating (in this case produced by deceleration of the flow in the inlet) or sampling…"

The authors are aware that CFD (if carried out properly) would be a good way to characterise the inlet system, but decided not to include any CFD because it is far beyond the scope of the PhD project of the main author and it is very unlikely that it would change the conclusions of the paper. In addition, we think that the use of the appropriate empirical equations in combination with the comparison with underwing optical probes is an effective means of determining the best method of using the inlet and what biases can be expected.

The section 8 and 9 appear as a misfit in the context of this technical paper. I suggest removing it here and extending it into a standalone paper or letter in another journal. A proof of capability of SEM and measurements with the filter system on board the aircraft is not really required, as this has been done during decades (Johnson et al.,1991; Formenti et al., 2003; Chou et al., 2008; Johnson et al., 2012). In addition, the plots are shown, but remain un-discussed, and no context (e.g., meteorology, trajectories, campaign aims) is given. If anything of the SEM compositional results should be included, I suggest including the sensitivity tests for the classification scheme as function of the detection limit (currently in the supplement), as from this you can derive recommendations with respect to element quantification settings.
We interpreted that this comments refers to the sections 7 and 8 (SEM compositional categories, and an example of an application).

Sensitivity tests have now been included in the main paper (Appendix C).
Sect. 7 (The Section regarding to the compositional categories) has been moved to the Appendix B, in order to make the paper flow better.

Sect. 8 (now Sect 6), which includes some examples of what the technique can do has been kept just as an example without further discussion since this is a techniques paper. Further publications including all the SEM data collected by the authors and its discussions are already in preparation, and they will refer to this publication, rather than describing the technique in multiples SI sections of these future publications. The SEM technique has been used by other parallel projects in ground collected samples, which will also refer to this work.
Add in Sect. 8: "The purpose of this section is purely to give examples of the capabilities of the technique, further analysis is planned for subsequent papers"

On the comment about the SEM technique being used in the past. Yes, it has been used in the past, but our approach draws on elements of a number of previous studies and the classification scheme is novel. It therefore needs to be described somewhere. Hence, we think this techniques paper is the perfect place to include this.

Detailed remarks / corrections
Abstract 28-30: While this is surely true, it's not part of the paper.
Removed

40 Missing "."
Corrected

55 "... has been limited." was not carried out?
Some efforts have been made, we reviewed these previously in Price et al. (2018), but they are very limited. We are more specific in section 8 where we refer to the relevant papers. We have added the relevant references to this statement in the introduction as well.

57-67: These lines are more a summary than an introduction. As it is partly redundant to section 9, I suggest removing it.
Yes, this paragraph is the summary of what will come in the paper. We usually structure our papers in this way since it helps focus in on the specific objectives of the paper.

88: It doesn't get clear from the picture: does the 0.7 cm inlet have the inner edges rounded? From the references literature I would think that it is.
The word curved has been added to the text, as done in the given references.

97: The numbers indicate a high precision, which is usually not achieved by mass flow meters (1 – 3 % uncertainty). How water vapour was treated, which influences the reading?
The uncertainty of the MFM has been added (See caption of Fig. 4). Since the error is 1 % of the full scale (and this one is 400 L/min), the errors are above 1%.

Water vapour was neglected, since its effect is negligible. The difference in the heat capacity of dry air and saturated air at 20 ºC is about 2%. The difference in the molar mass of dry air and saturated air at 25 ºC is about 1.2%.
Add in Sect. 2.2: "The presence of water vapour hasn't been corrected since its effect is negligible."

98: It probably reports the gas mass, not volume.
It measures the gas mass but reports the equivalent volume at standard conditions.

101: Rietschle?
Added in Sect. 2.1: Elmo Rietschle (Gardner Denver Inc.)

110: Particles are not necessarily lost (to the wall), but can be diluted (i.e. not entering the inlet).
It is not clear how aerosol would be diluted in this inlet.

112-113: and depending on pressure and temperature...?
Added to second paragraph of Sect. 2.2: "The sampling efficiency of any inlet depends on the flow rates, and the flow regime (laminar vs turbulent), the pressure and the temperature."

122: It seems that to rate the importance of a mechanism, its effect needs to be compared to all others. Was this done, or were the only most probably important mechanisms selected? Please explain the reasoning.

We have included and excluded the same mechanisms as described in von der Weiden et al. (2009) (the reference has been added to this line in the text).
Add in third paragraph of Sect. 2.2: (a discussion on the choice of equations, how they have been applied and the excluded mechanisms can be found in Appendix A)
Added in last paragraph of Appendix A: "Other losses: Some mechanisms (thermophoresis, diffusiophoresis, interception, coagulation and re-entrainment of deposited particles) have not been considered, since they are second order mechanisms under our conditions when compared with the calculated mechanisms (Brockmann, 2011; von der Weiden et al., 2009) and for one of them (electrostatic deposition) it is not possible to quantify them. Electrostatic deposition is normally avoided by using grounded conductive materials so no electrical field exists within the tubing (Brockmann, 2011). Since the FAAM BAe-146 research aircraft is not grounded during the flight, we cannot state this mechanism is irrelevant. However, the experimental agreement between the SEM and optical probes suggest that this is a minor loss mechnanism."

126-162: Too redundant with the appendix. Suggestion: either refer to the appendix and remove all short explanations here, or include the full discussion currently in the appendix. For a technical journal, also the latter would be appropriate.
Most of the explanations have been removed.

181-182: How does the bypass change the temperature in the inlet (probably mitigate heating by less deceleration)? Is the effect strong enough to impact on volatile particles?
The fact that it is not possible at all to have temperature and pressure measurements through the inlet system (for certification reasons) limits our understanding of the bypass system. We can only state qualitatively that, as you mention, they bypass will decrease heating trough less deceleration (and maybe removing some heat from the system).

213: It is somewhat surprising that the filter flow appears to be unregulated. Maybe, a regulation system should be included in future as well.
Yes, we are recommending this as a part of a mid-life upgrade of the FAAM aircraft.

217: "microscope"
Fixed

244: "highly unlikely" instead of "not likely"?
Added
262: "regarded" instead of "shown"?
Added

263: Regarding the "reference": just recently, there was a publication showing size distribution distortion for the 'free-stream' instruments, too, (Spanu et al., 2019), which might be worth checking.
Although we are aware that the probes might have some sampling biases, as stated in Rosenberg et al. (2012), we still decided to use them as a refernece, as in previous works (Chou et al., 2008; Young et al., 2016; Ryder et al., 2018; Price et al., 2018).

281: Kandler et al. used mostly backscatter electron, except for small particles on TEM grids. Check also the other references please.
Corrected, and all the references were checked and updated

284: Is it possible to quantify the undercounting of backscatter versus secondary electron? That might be valuable information for people dealing with similar questions.
We thought about it, however, this would be extremely dependent on the aerosol sample so we decided to state it in a qualitative way.

283-298: Can you include an image showing the benefit of the Ir coating and the potential size increase? Again that appears to be valuable information.
The only thing we could do is taking some carbon coated images of some areas and some Ir coated images of different areas of the same filter (we cannot take Carbon coated images of an area, recoat it with Ir and go to the same area to take more images). The comparison would also be dependent upon the specific settings of the

instrument, hence we feel that a qualitative statement that we found Ir to be a better coating material is warranted, but a more detailed comparison is not.

301-304: it appears to be more meaningful to specify the pixel size in nm (scanning grid size), instead of the magnifications, which are screen-related.
Done

310: Was the ECD converted into aerodynamic or optical equivalent diameter or just used "as it is"? Please discuss, as this might introduce certain biases.
Added in third paragraph of Sect. 4: "This equivalent circular diameter hasn't been corrected or transformed into an optical or other equivalent diameter"
Added to fourth paragraph of Sect. 5: "Disagreement in the measurements can be also produced by the fact that the techniques are measuring different diameters; (optical and geometric)"

316: "evenly": In Fig. 7, a min/max variation of a factor of three is visible, interestingly without a size bias. Was it the same in all radial directions, or is that random fluctuations?
Added to fourth paragraph of Sect. 4: "In Fig. 7 one can see the radial distribution of aerosol particles on top a filter collected using the inlet system. In spite of some fluctuations (which are up to a factor 3 and appear to be random), one can see that the particles are homogenously distributed all over the central ~30mm of the filter. The areas were chosen by the user from all over the surface of the selected fraction of the filter".

320: Please 'link' "ECD" to "equivalent circular diameter".
Done

322-323: Where these charging problems observed despite the relative thick Ir coating?
Added to fifth paragraph of Sect. 4: "This reduces the likelihood of image defocusing over the SEM automated run".

We observed a frequent image focusing problem during long overnight runs, when the filters we were scanning had large numbers (above 20) of particles per image. We performed some tests and long exposure to the electron beam seemed to be the only reason of this defocusing effect. After adding the 12-15 particle limitation, this defocusing as a consequence of beam exposure effect was mostly eliminated.

414-415: I suggest treating this more precisely. At 10 µm, there is a disagreement of about a factor of 10 or slightly more, and the theory predicts between 2 and 5. Considering the uncertainties, it's probably fair to call this agreement. At 2 µm, there is the same factor > 10 difference, but the theory says 1. Here, 'agreement' becomes stretched. However, the optical particle counter curves have persistent minima (3 µm, 10 µm) and maxima (2 µm, 5 µm), where the SEM curve is smooth. Are these minima/maxima realistic or potentially an artifact of a failing Mie inversion?

We would rather keep this discussion qualitative for several reasons, not least that we are contrasting optical sizes with geometric sizes and also that the flow rates in the theoretical calculations were not identical to those in these specific experiments. However, the qualitative conclusion that the bypass being open reduces the isokinetic enhancement is valid and this should be written more clearly. We have amended the line to read:

(Added to second paragraph of Sect. 5) "The results of these comparisons are in qualitative agreement with the theoretical calculations in Sect. 2.2, i.e. that the sub-isokinetic enhancement is reduced with the bypass open."

In addition we have stated why we do not make a quantitative comparison or use the theory to 'correct' the data:

Added to end of Sect. 5 "Given the uncertainties on both techniques and the fact that they measure different diameters (optical diameter in the case of the PCASP-CDP and geometric equivalent circular diameter in the case of the SEM), this comparisons cannot be used to quantify the biases in the system, but can be used to make a qualitative comparison. For similar reasons, the SEM data hasn't been corrected using the theoretical efficiency."

In addition, on reviewing section 5 in light of the referee's comments we decided to restructure it. We now present the information in a more logical manner, which reflects the order of the figures. Please refer to the revised section 5 for the changes.

479: “sulphate aerosol particles, which are solid or liquid sulphuric acid particles” If it is sulphate (probable), then it is a salt as reaction product from an acid with something else. Solid sulphuric acid on a filter is improbable. Please correct the phrasing. Also, particles in this category could be organo-sulphates.

Yes, this description was poor. We have replaced this text with the following (Appendix B3):
“Aerosol particles in this category contained a substantial amount of S. This S might be in the form of inorganic or organic sulphate compounds. Some sulphate compounds, such as sulphuric acid, are relatively volatile and will be lost in the SEM chamber.”

501: “chloride”. Potassium-rich Cl- (and/or S-) containing particles are known from biomass burning (Li et al., 2003; Lieke et al., 2011), and other Cl-rich from (waste) incineration (Willison et al., 1989; Graedel and Keene, 1995).
Added to Sect 7.5

512: How about fractionated crystallization of a sea-water droplet on the filter, leading to separate NaCl, MgCl, CaCO3 or CaSO4 particles?
Added to Appendix B6: “Some Ca rich particles could originate from the crystallization of sea water, loosely attached to NaCl. The latter component would dominate over the rest of the elements of the conglomerate and they would appear as Na rich particles, unless they shatter in the air (Parungo et al., 1986){Andreae, 1986 #503}(Hoornaert et al., 1996)”

648-650: This approach appears to be questionable, as turbulence for an increasing diameter tube probably has an additional generation mechanism (inertia), compared to turbulence in a constant diameter tube (mostly by shear). Please comment.
Added to appendix A: “This approach doesn’t account for potential additional inertial losses that could occur as a consequence of the enlargement of the flow in the conical section.”

However, the angle of enlargement is small (5.7º). It was designed to be below 7º in order to avoid flow separation (Andreae et al., 1988). In addition, the bending towards the wall that the particles could experience as a consequence of this 5.7º expansion is smaller than the bending towards the wall that the particles already have before entering the nozzle because of the sub-isokinetic expansion of the flow, which has already been quantified.

654-669: The bend approximation assumes a smooth tube, too. If it was used for the droplet separator, the conditions are not met. Also, if the flow is decelerated during the bend, large particles might become accumulated on the outer side, which is not accounted for by the simple approximation. Please discuss.
In Brockmann (2011) (page 94) they suggest to use this approach for flow constrictions such as a tee.

Add line: “This assumption might underestimate the losses since some large aerosol particles will become accumulated in the bypass”.

683: For diffusion a constant diameter bend can probably be well-approximated by a straight tube.
That is what we did. This is stated in Appendix A (9th paragraph).

691-703: While it is correct that the particles are retained by the filter, not necessarily all particle sizes can be analyzed by microscopy techniques (representatively), as the smaller particles might be deposited inside the pores, too.
Added in Appendix A (9th paragraph): “However, the fact that some aerosol particles with diameters below the pore size could be deposited in the filter pores and therefore not be detected by the SEM technique could contribute to the undercounting”.

707: The referred equations apply to sharp-edged nozzles, while in the setup blunt and probably rounded ones are used (according to the aircraft engine inlet description). In particular the inlet rounding is done to mitigate misalignment effects (Hermann et al.,2001).

The criteria of the classification appears again in Belyaev and Levin (1974), where they state that inlets which had certain ratios in between the diameters of the inlet edge, thickness and angles could be considered thin-walled or thick-walled. According to them, the problem with the thick-walled nozzles is that the air streamlines are

distorted when they approach the inlet edge. Belyaev and Levin (1974) state that the ratio in between the external and the internal diameter of the inlet edge must be below 1.1, but we cannot really define this parameter because of the curved profile of the edge. An alternative criteria is that the ratio in between the thickness of the inlet edge and the diameter of the edge is below 0.05. Again, it is not possible to define the thickness of the edge. The numerical criteria thin/thick walled seems to be designed for truncated conical sections, not for curved edges like our case.

However, the inlet we are considered has been designed to "avoid distortion of the pressure field at the nozzle tip and the resulting problems associated with flow separation and turbulence" (Andreae et al., 1988), and it has been described as thin-walled in the literature (Talbot et al., 1990; Andreae et al., 2000; Formenti et al., 2003), because this design that avoids flow separation and turbulence places it closer to the "thin-walled" category than the "thick-walled" category. As a consequence, we decided to apply the thin-walled equations to it.

The fact that the experimental data shows the same trends in the inlet behaviour than predicted using the thin wall assumption helps to strengthen this assumption.

A short explanation of this has been added to the text (Fourth paragraph of Appendix A).

924: Caption "Polycarbonate". As many effects discussion above might be closer related to the volumetric flow rate than to the mass flow rate, it should be shown in addition. The Iceland/Cape Verde ratio is inverted for the two filter types or two inlet types. How can this be explained?
It is true that for the polycarbonate case, the Cape Verde sampling was consistently about 10 L min-1 above the Icelandic sampling. However, we don't believe there is enough Icelandic samples to say there is an inverse trend for the Teflon case.

References

Andreae, M.O., Berresheim, H., Andreae, T.W., Kritz, M.A., Bates, T.S. and Merrill, J.T. 1988. Vertical-Distribution of Dimethylsulfide, Sulfur-Dioxide, Aerosol Ions, and Radon over the Northeast Pacific-Ocean. *Journal of Atmospheric Chemistry.* **6**(1-2), pp.149-173.

Andreae, M.O., Elbert, W., Gabriel, R., Johnson, D.W., Osborne, S. and Wood, R. 2000. Soluble ion chemistry of the atmospheric aerosol and SO2 concentrations over the eastern North Atlantic during ACE-2. *Tellus B.* **52**(4), pp.1066-1087.

Belyaev, S.P. and Levin, L.M. 1974. Techniques for collection of representative aerosol samples. *Journal of Aerosol Science.* **5**(4), pp.325-338.

Brockmann, J.E. 2011. Aerosol Transport in Sampling Lines and Inlets. *Aerosol Measurement.* John Wiley & Sons, Inc., pp.68-105.

Chou, C., Formenti, P., Maille, M., Ausset, P., Helas, G., Harrison, M. and Osborne, S. 2008. Size distribution, shape, and composition of mineral dust aerosols collected during the African Monsoon Multidisciplinary Analysis Special Observation Period 0: Dust and Biomass-Burning Experiment field campaign in Niger, January 2006. *Journal of Geophysical Research Atmospheres.* **113**(D17), pp.1-17.

Formenti, P., Elbert, W., Maenhaut, W., Haywood, J. and Andreae, M.O. 2003. Chemical composition of mineral dust aerosol during the Saharan Dust Experiment (SHADE) airborne campaign in the Cape Verde region, September 2000. *Journal of Geophysical Research.* **108**, p8576.

Hoornaert, S., Van Malderen, H. and Van Grieken, R. 1996. Gypsum and Other Calcium-Rich Aerosol Particles above the North Sea. *Environmental Science & Technology.* **30**(5), pp.1515-1520.

Parungo, F.P., Nagamoto, C.T. and Harris, J.M. 1986. Temporal and spatial variations of marine aerosols over the Atlantic Ocean. *Atmospheric Research.* **20**(1), pp.23-37.

Price, H.C., Baustian, K.J., McQuaid, J.B., Blyth, A., Bower, K.N., Choularton, T., Cotton, R.J., Cui, Z., Field, P.R., Gallagher, M., Hawker, R., Merrington, A., Miltenberger, A., Neely Iii, R.R., Parker, S.T., Rosenberg, P.D., Taylor, J.W., Trembath, J., Vergara-Temprado, J., Whale, T.F., Wilson, T.W., Young, G. and Murray, B.J. 2018. Atmospheric Ice-Nucleating Particles in the Dusty Tropical Atlantic. *Journal of Geophysical Research: Atmospheres.* **123**(4), pp.2175-2193.

Rosenberg, P.D., Dean, A.R., Williams, P.I., Dorsey, J.R., Minikin, A., Pickering, M.A. and Petzold, A. 2012. Particle sizing calibration with refractive index correction for light scattering optical particle counters and impacts upon PCASP and CDP data collected during the Fennec campaign. *Atmospheric Measurement Techniques.* **5**(5), pp.1147-1163.

Ryder, C.L., Marenco, F., Brooke, J.K., Estelles, V., Cotton, R., Formenti, P., McQuaid, J.B., Price, H.C., Liu, D.T., Ausset, P., Rosenberg, P.D., Taylor, J.W., Choularton, T., Bower, K., Coe, H., Gallagher, M., Crosier, J., Lloyd, G., Highwood, E.J. and Murray, B.J. 2018. Coarse-mode mineral dust size distributions, composition and optical properties from AER-D aircraft measurements over the tropical eastern Atlantic. *Atmospheric Chemistry and Physics.* **18**(23), pp.17225-17257.

Seinfeld, J.H. and Pandis, S.N. 2006. *Atmospheric Chemistry and Physics: From Air Pollution to Climate Change.* Wiley.

Talbot, R.W., Andreae, M.O., Berresheim, H., Artaxo, P., Garstang, M., Harriss, R.C., Beecher, K.M. and Li, S.M. 1990. Aerosol Chemistry during the Wet Season in Central Amazonia - the Influence of Long-Range Transport. *Journal of Geophysical Research Atmospheres.* **95**(D10), pp.16955-16969.

Trembath, J. 2012. *Airborne CCN Measurements, Doctor of Philosophy*. thesis, University of Manchester.

von der Weiden, S.L., Drewnick, F. and Borrmann, S. 2009. Particle Loss Calculator – a new software tool for the assessment of the performance of aerosol inlet systems. *Atmospheric Measurement Techniques.* **2**(2), pp.479-494.

Young, G., Jones, H.M., Darbyshire, E., Baustian, K.J., McQuaid, J.B., Bower, K.N., Connolly, P.J., Gallagher, M.W. and Choularton, T.W. 2016. Size-segregated compositional analysis of aerosol particles collected in the European Arctic during the ACCACIA campaign. *Atmospheric Chemistry and Physics.* **16**(6), pp.4063-4079.

Responses to Referee 2 (R2)

This paper presents a characterization of the filter inlet system of the research aircraft BAe146. It includes calculated inlet sampling and transmission efficiency, a description of the analysis of the filter samples by scanning electron microscopy (SEM), and a comparison of the size distributions obtained by SEM with underwing aerosol and cloud probes.

Unfortunately, the manuscript suffers from being vague at important points. Especially for a technical journal, a comparison between calculations and measurements needs to discussed in more detail. Also, expressions like "in agreement" are used frequently where a precise numbers (with error limits) would have been necessary. Thus, I cannot recommend publication in the current stage and suggest some major revision before publication.

Major points:
As said above, the manuscript lacks precise numbers. Many statements are vague, like "in agreement" or "minor fraction" etc. This is not sufficient for a technical journal.

We have amended Sect. 4 and in Sect. 5 in order to remove subjective statements where possible and replace them with more quantitative statements.

Furthermore, the SEM part is a description of the classification, but no further validation is done. Additional aircraft-based gas (e.g. CO) and particle measurements (mass spectrometers?) may help to characterize the air mass origin and the particle properties and thereby validate the composition.

We gave this some thought when planning these experiments, but concluded that it was not possible to find an established technique that we could quantitatively validate our SEM technique against. Validation of the size resolved composition would require significantly more detailed particle by particle information than could be inferred from tracers like CO or even from the available aerosol mass spectrometers. The AMS for example only provides information on the non-refractory components of fine mode aerosol.

In order to address the comment we have included a new figure (Fig 11) where we show an additional six size resolved compositions. This is accompanied by a new discussion in Sect. 6. Sect. 6 now focuses on examples and the paragraph on mass spec techniques has been removed. Fig. 7 includes data for SE England and Alaska (three samples for each). The extremely good agreement between the Figure 11c and 10a, which were samples from the same flight, helps to demonstrate the reproducibility. We also, show that the composition of the aerosol in the two locations is different in ways which we would expect, which shows that we are sensitive to different aerosol types and the composition varies in a consistent way.

Of course, the ideal situation would be to have a standard instrument to compare against, but given this standard instrument does not exist, we suggest that the best way forward would be to take part in a suitable inter-comparison at some point in the future.

The comparison of SEM size distribution with the PMS probes is not very conclusive, because only qualitative statements ("in good agreement") are made.
The discussion of the SEM-Optical probes (Sect. 5) comparisons has been restructured and improved.

Furthermore, the size distributions of the PCASP (Fig. 5) seem to have a problem at 300 nm and above 2 _m. The PCASP shows decreasing number concentrations above 2 _m while the CDP starts at 5 _m with much higher number concentrations. Does the PCASP underestimate particle number above 2 _m? If so, would it be better to omit these points and use a lognormal fit to the reliable CDP and PCASP data to obtain realistic fine and coarse mode distributions? To what extend can such size distributions validate the inlet efficiency if the uncertainties are so high?

Unfortunately there were some errors in Fig 5, which have now been corrected. Nevertheless, we sometime see an apparent discrepancy between the PCASP and CDP at above 2 um (the discrepancy at 300 nm is resolved using the correction detailed in Rosenberg et al. (2012) which is already discussed in the text (we accidently plotted the uncorrected data). In addition, horizontal error bars have been added to all the PCASP-CDP data.

In the reference paper for the PCAS_CDP calibration, one can read: "Some bumps seen in the PCASP distribution have been accentuated by the calibration and refractive index correction presented here. It could be the case that these are real modes or there is the potential that this is an artefact caused by imperfect knowledge of the particle scattering properties" (Rosenberg et al., 2012). Hence, it is very difficult to address if the feature at 2 um is physical or just an artefact. However, in other data (Fig 8b, Fig 9a, b and c), these bumps cannot be seen as easily and in all the cases as in Fig 5 (which is the same data as Fig 8a), so they are likely to be physical.

Added to end of Sect. 5: "Some of the PCASP size distributions contain some bumps (above 2 μm), but it is not possible to address if they are physical or just an artefact produced by the calibration (Rosenberg et al., 2012)."

We strongly disagree that it is a good idea to show fits for the comparisons instead of the data with errors. The fitting can have some subjective parameters (number of modes and restrictions on the fit) and not showing the actual data would potentially omit a lot of information. As a consequence we decided to keep only the data without any fitting on it and understand the uncertainties and potential artefacts of the system. In addition, Rosenberg et al. (2012) does not recommend showing a fit instead of the data as a way to deal with the bumps.

Figure 8-10: Have the SEM data been corrected for the calculated inlet transmission and aspiration efficiency? I could not find a statement on this in the text. If not, then an overestimation of about a factor 3 - 4 around 10 _m should be observed (from Fig 3b). Is that the case? By bare eye, the factor seems to be larger than three, but there is no discussion in the text, except for a "good agreement" statement.

We do not correct the data for the inlet efficiency. This is now clearly stated in the text (fifth paragraph of Sect 5):

"Given the uncertainties on both techniques and the fact that they measure different diameters (optical diameter in the case of the PCASP-CDP and geometric equivalent circular diameter in the case of the SEM), this comparisons cannot be used to quantify the biases in the system, but can be used to make a qualitative comparison. For similar reasons, the SEM data hasn't been corrected using the theoretical efficiency"

The referee refers to a factor of 3-4 enhancement. Based on the calculations we recommend that sampling is performed with total flow rates greater than 50 L min^{-1} with the bypass open, which result in enhancement smaller than about a factor of 2.

Regarding the 'good agreement' comment, we have made an effort to be more quantitative throughout the manuscript, particularly in discussion of the size distributions. We have reorganised section 5, also in light of the other referee's comments.

Minor

I was a bit confused by the mixture of sampling efficiency study and chemical composition study. I see that both needs to be done, but I needed some time to realize that the manuscript focuses on these two topics. Maybe a change of the title would help the reader.

Both aspects of the study are mentioned in the title, so it is not clear how we would change it to make it clearer. We reinforce this in the abstract and also in the (revised) final paragraph of the introduction.

Specific comments

Line 353: "This happens more frequently for smaller particles, but it can also happen with some larger particles..." What is "smaller" and "larger" here? Please be more precise and give a size range.

Done.

Added to 6th paragraph of Sect 4.

Line 366-368: "The number of particles is very low, typically about the order of magnitude of one particle per 100 by 100 _m square, which is well below the typical particle loading on a filter exposed to the atmosphere" Please give numbers for typical particle loading. "Well below" is not quantitative.

Added to end of Sect. 4: "The number of particles is typically about the order of magnitude of one particle per 100 by 100 μm square, which is more than an order of magnitude below all the samples in this study (apart from the sample shown in Fig 9c, where it is only about a factor 2)"

Line 373: "...from the analysis of atmospheric aerosol (it was only ever a very minor component)." Please specify "very minor".

Sentence was deleted for simplicity. The only purpose of the explanation was stating that that element is not very necessary for most of the aerosol studies.

Line 374: "By doing this, we make sure that we excluded more than half of the artefacts of the analysis" I don't understand. Before that, you said that >90% contained Cr, so you would remove >90 of the artefact, isn't it?

Now it has been better explained:

Added to end of Sect. 4: "In Fig. S2 one can see that about half of particles found in both blank filters and the handling blank belong to the metallic rich category. However, further examination of the composition of these metal rich particles revealed that almost all of them were Cr rich particles (about 97 % in the case of the blank filters and about 96% in the case of the handling blank). As a consequence, we excluded all the Cr rich particles from the analysis of atmospheric aerosol. By doing this, we make sure that we exclude about half of the artefacts of the analysis"

Section 7. Did you observe any signs of meteoric material (see Murphy et al., 2014)? Particles dominated by Fe, Mg, Si and S ?

Although we did observe particles dominated by these elements, we cannot conclude that they are meteoric material since most of them were taken in the troposphere (most of them in the first kilometre), rather than the stratosphere where meteoric material has been observed. Analysis of meteoric material with the SEM seems more complicated since it only provides the weight percentages of the elements in the aerosol particles without any information about the isotope or the mass to charge ratio of what it is in the sample, but we will consider this while analysing the composition data which will be included in future papers.

Line 501: "sodium chlorine" -> sodium chloride

Done

Fig 4, caption: "FAAM core datasets" have not been explained before:

Added to first paragraph of Sect. 3: "All the PCASP-CDP data shown here has been extracted from the FAAM cloud datasets corresponding to each specific flight via the Centre for Environmental Data Analysis"

Added to caption of Fig. 4: "The altitude data was extracted from the FAAM core datasets C019, C022, C024, C025, C058, C059, C060, C061, C062, C063, C085, C086, C087, C088, C089, C090 and C091 (via the Centre for Environmental Data Analysis)"

Fig 5 + lines 257-264: As already written above, the size distributions of the PCASP (Fig. 5) seem to have a problem at 300 nm and above 2 _m. The PCASP shows decreasing number concentrations above

2 _m while the CDP starts at 5 _m with much higher number concentrations. Does the PCASP underestimate particle number above 2 _m? If so, would it be better to omit these points and use a lognormal fit to the reliable CDP and PCASP data to obtain realistic fine and coarse mode distributions? What happens at 10 _m with the CDP?

We addressed the first points above.
In most cases, the CDP counting decreases around 10 um, but this is likely to be an actual measurement and not an artefact since particles above those sizes are relatively rare in the atmosphere.

Figs 8 and 9: I suggest combining Figs 8 and 9 into one figure with 4 graphs.
Done

Fig 8, 9, 10 and line 415: "The results of these comparisons are in agreement with the theoretical calculations in Sect. 2.2." Did you correct the SEM size distribution with the calculated sampling efficiency? Can you divide SEM dN / PMS dN and derive an "experimental" sampling efficiency and compare that to the calculated curves in Sect. 2.2? One of the above should be done, otherwise your statement "are in agreement" is too weak.

We regard the efficiency calculations as qualitative, i.e. they provide a qualitative indication of losses and how to best use the inlet while minimising sampling biases. We therefore cannot use them to 'correct' the data, doing so would likely introduce a unquantifiable error to the data.

Added to end of Sect. 5: "Given the uncertainties on both techniques and the fact that they measure different diameters (optical diameter in the case of the PCASP-CDP and geometric equivalent circular diameter in the case of the SEM), this comparisons cannot be used to exactly quantify the biases on the system but understand its presence. For similar reasons, the SEM data hasn't been corrected using the theoretical efficiency"

References

Rosenberg, P. D., Dean, A. R., Williams, P. I., Dorsey, J. R., Minikin, A., Pickering, M. A., and Petzold, A.: Particle sizing calibration with refractive index correction for light scattering optical particle counters and impacts upon PCASP and CDP data collected during the Fennec campaign, Atmos. Meas. Tech., 5, 1147-1163, 2012.

Manuscript

Characterisation of the filter inlet system on the BAE-146 research aircraft and its use for size resolved aerosol composition measurements

Alberto Sanchez-Marroquin[1], Duncan H. P. Hedges[1], Matthew Hiscock[2], Simon T. Parker[3], Philip D. Rosenberg[1], Jamie Trembath[4], Richard Walshaw[1], Ian T. Burke[1], James B. McQuaid[1], Benjamin J. Murray[1]

[1]School of Earth and Environment, University of Leeds, Woodhouse Lane, Leeds, LS2 9JT, UK

[2] Oxford Instruments NanoAnalysis, High Wycombe, HP12 3SE

[3]Defence Science and Technology Laboratory, Salisbury, SP4 0JQ, UK

[4]Facility for Airborne Atmospheric Measurements, Building 146, Cranfield University, College Road, Cranfield, Bedford MK43 0AL

Abstract

Atmospheric aerosol particles are important for our planet's climate because they interact with radiation and clouds. Hence, having characterised methods to collect aerosol from aircraft for detailed offline analysis are valuable. However, collecting aerosol, particularly coarse mode aerosol, onto substrates from a fast moving aircraft is challenging and can result in both losses and enhancement in particles. Here we present the characterisation of an inlet system designed for collection of aerosol onto filters on board the Facility for Airborne Atmospheric Measurements (FAAM) BAe-146 research aircraft. We also present an offline Scanning Electron Microscopy (SEM) technique for quantifying both the size distribution and size resolved composition of the collected aerosol. We use this SEM technique in parallel with online underwing optical probes in order to experimentally characterise the efficiency of the inlet system. We find that the coarse mode aerosol is sub-isokinetically enhanced, with a peak enhancement at around 10 µm up to a factor of three under typical operating conditions. Calculations show that the efficiency of collection then decreases rapidly at larger sizes. In order to minimise the isokinetic enhancement of coarse mode aerosol we recommend sampling with total flow rates above 50 L min^{-1}; operating the inlet with the bypass fully open helps achieve this by increasing the flow rate through the inlet nozzle. With the inlet characterised, we also present single particle chemical information obtained from X-ray spectroscopy analysis which allows us to group the particles into composition categories.

Deleted: UK's

Deleted: Facility for Airborne Atmospheric Measurements (FAAM)

Deleted: . Our intention is to use the composition information in parallel with filter based ice nucleating particle measurements in order to correlate composition and ice nucleating particle concentrations.¶

Page Break

1 Introduction

Atmospheric aerosol particles are known to have an important effect on climate through directly scattering or absorbing solar and terrestrial radiation as well as through indirect effects such as acting as Cloud Condensation Nuclei (CCN) or Ice-Nucleating Particles (INPs) {Albrecht, 1989 #403;Haywood, 2000 #404;DeMott, 2010 #406;Hoose, 2012 #317;Lohmann, 2017 #409;Lohmann, 2006 #582}. Aerosol particles across the fine (diameter < 2 µm) and coarse (> 2 µm) modes are important for these atmospheric processes. For example, aerosol in the accumulation mode are important CCN {Seinfeld, 2006 #473}, whereas supermicron particles are thought to contribute substantially to the INP population {Pruppacher, 1997 #594;Mason, 2016 #595}{Creamean, 2018 #604}. Hence, being able to sample across the fine and coarse modes is required to understand the role aerosol play in our atmosphere. However, sampling aerosol particles without biases can be challenging, this being especially so on a fast moving aircraft {Wendisch, 2013 #501;McMurry, 2000 #411;Baumgardner, 1993 #413;Baumgardner, 2011 #596}.

It is necessary to sample aerosol from aircraft because in many cases aircraft offers the only opportunity to study aerosol and aerosol-cloud interactions at cloud relevant altitudes {Wendisch, 2013 #501}. However, the relatively high speeds involved present a set of unique challenges for sampling aerosol particles. This is especially so for coarse mode aerosol which are prone to both losses as well as enhancements because their high inertia inhibits their ability to follow the air stream lines when they are distorted by the aircraft fuselage and the inlet {McMurry, 2000 #411;von der Weiden, 2009 #325;Brockmann, 2011 #344}. Therefore, inlet design and characterisation becomes extremely important when sampling aerosol particles.

In this study we characterise the inlet system used for collecting filter samples (known as the Filters system) on board the UK's BAe-146-301 Atmospheric Research Aircraft, Facility for Airborne Atmospheric Measurements (FAAM). This system has been used for many years, but its characterisation has been limited {Chou, 2008 #447}{Young, 2016 #75;Price, 2018 #450}{Ryder, 2018 #541}. Our goal in this characterisation work was to define recommendations for the use of the inlet system to minimise sampling biases and define the size limitation and the biases that exist. While the filter samples could be used for a variety of offline analyses, we have done this characterisation with two specific goals in mind: firstly, we want to use this inlet system for quantification of INP (the technique for this analysis has been described previously {Price, 2018 #450} and will not be further discussed here); secondly, we have adapted and developed a technique for quantification of and the size resolved composition of the samples using Scanning Electron Microscopy (SEM). We use this technique in order to test the inlet efficiency. These experiments are underpinned by calculations which elucidate how the biases are impacted by variables such as flow speed, angle of attack and use of the bypass system. Finally we present an example of the use of the inlet for determining the size resolved composition of an aerosol sample collected from the FAAM aircraft.

Deleted: research aircraft

Deleted: .

Deleted:

Deleted: size distributions and

Deleted: the SEM derived size distributions in comparison with the size distributions obtained from the underwing probes to experimentally

2. Description and theoretical sampling characteristics of the filter inlet system on the Facility for Airborne Atmospheric Measurements (FAAM) aircraft

Ideally, aerosol particles would be sampled through inlets without enhancement or losses. However, this is typically not the case when sampling from aircraft, hence it is important to know how the size distribution of the aerosol particles is affected by the sampling. Generally, an aircraft moves at high velocities with respect to the air mass that it is being sampled. During sampling on the FAAM aircraft the indicated airspeed is 100 m s^{-1}, which yields to a true airspeed that fluctuates between 100 and 120 m s^{-1}. The air mass has to decelerate when passing through the inlet {Baumgardner, 1993 #413} and this tends to result in inertial enhancement of coarse mode aerosol. There are also losses through the inlet system, for example, through inertial impaction at bends or gravitational settling in horizontal sections of pipework. These inlet characteristics need to be considered if the subsequent analysis of the aerosol samples is to be quantitative. In this section we first describe the existing inlet system and then present theoretical calculations for the size dependent losses and enhancements.

2.1 Description of the Filters system

The FAAM BAe-146 aircraft has two identical inlets for sampling aerosol onto filters for offline analysis. This inlet system was used to sample aerosol particles on board of the C-130 aircraft before being installed on the FAAM BAe-146 {Andreae, 1988 #296;Talbot, 1990 #453;Andreae, 2000 #294}, and it has been used to sample aerosol particles on the FAAM Bae-146 e.g. {Chou, 2008 #447;Young, 2016 #75;Price, 2018 #450;Hand, 2010 #444}. A diagram of the inlet system can be seen in Fig. 1. The two parallel inlet and filter holder systems, which each have a nozzle whose curved leading edge profile follows the criteria for aircraft engine intakes at low Mach numbers (low speeds when compared with the speed of sound; for FAAM during sampling this is ~0.3), and it is designed to avoid the distortion

of the pressure field at the end of the nozzle, flow separation and turbulence {Andreae, 1988 #296}{Talbot, 1990 #453}. The inlet has a bypass to remove water droplets or ice crystals through inertial separation and also enhance the flow rate at the inlet nozzle {Talbot, 1990 #453}. The flow through the bypass (bypass flow) can be regulated using a valve and it is driven passively by the pressure differential between the ram pressure inlet and the Venturi effect on the exhaust. After turning inside the aircraft, the airstream containing the aerosol particles continue through the filter stack after passing a valve. The air flow through the filter (filter flow) is measured by a mass flow meter, which measures the sampled air mass and reports it in equivalent liters at standard conditions (273.15 k, 1013.529 hPa). The uncertainty for this flow meter is 1% of the full scale (400 L min^{-1}). The effect of water vapour on the mass flow has not been corrected since its effect is negligible. The signal is integrated by an electronics unit to give the total volume of air sampled for any given time period. There is also a valve between the pump and the flow meter. The valve allows the inlet and pump to be isolated from the filter holder when changing the filter. The system uses a double-flow side channel vacuum pump model SAH55 made by Elmo Rietschle (Gardner Denver Inc.), aided by the ram effect of the aircraft. The flow rate at the inlet nozzle (total flow) is the sum of the bypass flow and the filter flow. The inlet nozzle is located at 19.5 cm of the aircraft fuselage, so the sampling is carried out in the free stream, outside the boundary layer.

Deleted: presence

Deleted: ’

2.2 Sampling efficiency

We present theoretical estimates of the losses and enhancements due to aspiration, inlet inertial deposition, turbulent inertial deposition, inertial deposition in bends and gravitational effects in Fig 2a. We used the term ‘efficiency’ to define the ratio between the number concentrations of particles after they were perturbed relative to the unperturbed value. If the efficiency is above one, the number of particles is enhanced whereas if it is below 1, particles are lost before they reach the filter.

Deleted: or diluted

The sampling efficiency of any inlet depends on the flow rates and the flow regime (laminar vs turbulent), the pressure and the temperature. Filter flow rates for 0.4 µm polycarbonate filters normally vary between 10 and 50 L min^{-1} depending on altitude (see section 2.3 for a discussion of flow rates). The bypass flow rate (when it is fully open) can go up to 35 L min^{-1} at 30 m and 22 L min^{-1} at 6 km (volumetric L at standard conditions: 273.15 k, 1013.529 hPa), but it is not measured routinely. In the 2.5 cm diameter section of the inlet, just after the inlet nozzle, the Reynolds number (Re) is below the turbulent regime threshold (Re > 4000) for flow rates below 65 L min^{-1}. For larger values of Re, the flow starts becoming turbulent. At the inlet nozzle, where the diameter 0.7 cm, Re is above 4000 for flow rates above 20 L min^{-1}, so the flow is briefly in the turbulent regime at the inlet for most sampling conditions. Fully characterising the losses and enhancements of aerosol particles passing through the inlet is very challenging since there are several aerosol size dependent mechanisms that can enhance or diminish the amount of aerosol particles that arrive at the filter.

Deleted: strongly

Deleted: than

Here we have considered the most important of these mechanisms {von der Weiden, 2009 #325} in order to estimate the inlet efficiency (see Fig. 2a) for a total flow rate of 50 L min^{-1} (all the flow rates of our calculations are given in L min^{-1} at standard conditions: 273.15 k, 1013.529 hPa). These loss mechanisms and their importance in this inlet system are defined as follows (a discussion on the choice of equations, how they have been applied and the excluded mechanisms can be found in Appendix A):

Aspiration efficiency has been calculated using the empirical equation as develop in {Belyaev, 1972 #499@@author-year} and {Belyaev, 1974 #498@@author-year}. As one can see in Fig. 2a this

Deleted: accounts for the fact that the speed of the sampled air mass (U_0) and the speed of the air through the beginning of the inlet nozzle (U) are different. In the case of the filter inlet system on the FAAM aircraft, the speed of the air mass is greater than the speed through the inlet (sub-isokinetic conditions), which leads to an enhancement of larger aerosol particles. Here, we have

mechanism enhances aerosol particles, tending to 1 for small diameters and to the ratio in between the air speed inside the nozzle and outside the aircraft for large ones.

Inlet inertial deposition has been characterised using the equation given in {Liu, 1989 #458@@author-year} which quantifies this effect. In Fig. 2a one can see that it produces some losses, with a minimum efficiency of down to 50% for sizes about 6 µm, without affecting the lower and upper limit of the aerosol size.

Turbulent inertial deposition occurs throughout the whole inlet system for flow rates above 65 L min^{-1} and only occurs in the inlet nozzle for flow rates below this threshold. We have used the equation given by {Brockmann, 2011 #344@@author-year} in order to account for this mechanism. In Fig. 2a one can see an example of the turbulent inertial losses at the nozzle. This mechanism gradually decreases the efficiency for aerosol particles above 5 µm.

Bending inertial deposition has been characterised using the equation given in {Brockmann, 2011 #344}. This efficiency mechanism, which can be seen in Fig. 2a, adds a size cut off with a D50 value at ~25 µm.

Gravitational settling of aerosol particles was considered using the equations developed in {Heyder, 1977 #466@@author-year} and {Thomas, 1958 #465@@author-year}, as stated in {Brockmann, 2011 #344@@author-year}. This efficiency mechanism adds another size cut off with a D50 value of 35 µm, as one can see in Fig. 2a.

Diffusional efficiency and filter collection efficiency have not been included in Fig. 2. The first mechanism has been calculated using the analytical equation given by {Gormley, 1948 #468@@author-year}, but it is not shown since it is very close to 1 for all the considered size range. For the filter types and pore sizes we used, filter collection efficiency is also close to a 100% across the relevant size range {Lindsley, 2016 #415;Soo, 2016 #462}.

Anisoaxial losses are losses produced by the fact that the inlet is not aligned with the velocity of the air mass, being offset by an angle, θ (related to the angle of attack). The anisoaxial sampling can affect the sub-isokinetic efficiency, but using the equations given by {Hangal, 1990 #534@@author-year}, we calculated that this effect is minimal for our conditions. In addition, anisoaxial sampling can lead to inertial losses when particles impact the inner walls of the inlet. This phenomena has been quantified using the equations in {Hangal, 1990 #535@@author-year} and the results can be seen in Fig. 3. As one can see, this efficiency mechanism adds an additional cut off for large aerosol particles (with values of D50 down to ~20 µm), depending on the value of the sampling angle.

One can see all the efficiency mechanisms combined for four different flow rates in Fig. 2b. These have been derived by multiplying all the efficiencies for the individual mechanisms. This overall efficiency is the ratio between the particles that reach the filter and the particles in the ambient air. The sampling efficiency for the submicron aerosol is close to 1. At sizes above 1 µm, the different loss mechanisms become increasingly significant. For the range of flow rates considered, the efficiency approaches zero between 20 and 50 µm, with D50 values in between ~13 and ~33 µm (although these values could be lower under certain values of angles of attack if considering the anisoaxial losses of from Fig. 3, which haven't been included). For the 80 L min^{-1} case, the flow is turbulent through all the pipe, leading to enhanced losses of coarse aerosol particles which partially compensate the sub-isokinetic enhancement of the system.

One can also see that the sub-isokinetic enhancement of large aerosol particles increases when decreasing the flow rate of the system. This effect is about a factor 3.5 for 10 µm particles when

Deleted: U/U_0

Deleted: is the inertial loss of aerosol particles within the nozzle because the flow expands inside the nozzle and the trajectory is therefore bent towards the wall. It

Deleted: happens when some particles are collected by the wall due to turbulences in the system. In our case, this

Deleted: , which can be seen in

Deleted: of aerosol particles is important in this inlet system at the 45º bend, where some particles are not able to follow air streamlines at bend. We have

Deleted: these losses

sampling at 15 L min^{-1}, but only a factor of two at 50 L min^{-1}. The sub-isokinetic enhancement can be mitigated using the bypass, which enhances the flow through the nozzle. This can be seen in Fig. 2c where one can see a comparison between the total efficiency of a 20 L min^{-1} flow rate through the filters with no bypass flow and the same case when the bypass is open. Since the considered bypass flow is comparable to the flow rate through the filters, the difference between the total flows for the two cases is approximately a factor 2. As a consequence, the maximum sub-isokinetic enhancement of large aerosol particles is almost a factor 2 larger when sampling with the bypass closed. Hence, the sub-isokinetic enhancement can be reduced by keeping the bypass fully open.

2.3 Sampling flow rate

Here we show flow rate data from four field campaigns in order to examine how the flow rate of the filter inlet system varied based on different factors. We have used the data collected during the ICE-D campaign, in Cape Verde during August 2015 {Price, 2018 #450}. The rest of the data is from some flight test carried out during 2017 and 2018, and three field campaigns. The first one was EMERGE, based in south east England, in July 2017. The second one was VANAHAEIM, based in Iceland in October 2017. The last campaign was MACSSIMIZE, based in Alaska in 2018. The flow rate of the inlet system is known to vary with altitude, with a lower flow rate at high altitudes because of the reduced pressure differential across the filter and the fact that the pump efficiency decreases at low pressure. In addition, it changes depending on the filter type and the pore size.

In Fig. 4, where all the flow rate data has been presented, one can see that the flow rate tends to decrease with altitude and change with filter type as expected, but the flow rates are not always consistent for each altitude and filter type, varying up to a factor two for each filter type/line/altitude/campaign. The filter type effect on flow rate can be seen in Fig. 4, where the average flow rate for 0.4 µm polycarbonate filters is about twice the flow rate of the 0.45 µm PTFE filters. In order to investigate the inconsistency in the flow rate at each altitude, we analysed the flow rate data by comparing it with different parameters (ambient air and cabin temperature, ambient air and cabin pressure, wind direction and speed with respect to the aircraft movement), but there was no correlation with any of these variables. Different mesh supports were used, but this does not affect the flow rate significantly according to some ground based tests. We checked the flow rate through each sampling period and found it did not change over time on a particular filter set (even after stopping the sampling and starting it again). In addition, we performed some tests on the ground and during flights to study the effect of potential leaks by inserting paper disks of the same dimension as the filters in the filter holders and found no evidence of leaks in the system.

We conclude that this variability in the flow rate comes from variability in the pump performance in combination with subtle differences in individual filter pairs. The side displacement pump is not the ideal pump for this system and operates at its maximum capacity. Hence, we suggest that to improve the performance of the system that flow rates are actively controlled and also the side displacement pump is replaced with a more appropriate design. This would also have the advantage that flow rates would be maintained at smaller pressure drops and allow sampling at higher altitudes.

3. FAAM underwing optical particle counters

Later in the paper we compare results from the underwing optical particle counters with our electron microscope derived size distributions, hence we describe the optical instruments here. The FAAM BAe-146 aircraft operates underwing optical particle counters to measure aerosol size distributions. These

include the Passive Cavity Aerosol Spectrometer Probe 100-X (PCASP) and the Cloud Droplet Probe (CDP). The PCASP measures particles with diameters in the approximate range 0.1-3 µm and the CDP measures the particles with diameters in the range of 2-50 µm. These instruments are placed outside the aircraft fuselage, below the wings. These instruments and the methods for calibration are described in {Rosenberg, 2012 #456}. All the PCASP-CDP data shown here has been extracted from the FAAM cloud datasets corresponding to each specific flight via the Centre for Environmental Data Analysis.

The instruments were calibrated and had optical property corrections applied as per {Rosenberg, 2012 #456@@author-year}. We used a refractive index of 1.56 + 0i and a spherical approximation (Mie theory) in the optical property corrections. In Fig. 5, one can see a sensitivity test on the refractive index value we used in order to examine how variability in refractive index affect the bin centres position, their width, and therefore the size distribution obtained from the PCASP and CDP. As one can see in Fig. 5a, modification of the real part of the refractive index from 1.5 to 1.7 can change the position of the PCASP bin centres up to a factor 1.5, but its effect on the CDP is not significant. When varying the imaginary part of the refractive index from 0 to 0.01, the bin centre positions of the first half of the range of the PCASP and CDP do not change but it can change the position of the bins of the end of the range of both instruments (less than a factor 1.5). However, for the purposes of this work, the differences produced by the variation in the refractive index are not large enough to modify the conclusions of the analysis, therefore we use a value of 1.56 + 0i.

The chosen refractive index range for this sensitivity analysis can be justified on the basis that the SEM compositional analysis showed that the composition of the aerosol samples used in this study was very heterogeneous, dominated by carbonaceous particles (biogenic, organic and black carbon) and with some contributions of mineral dust and other particle types. Values of the real part of the refractive index in the 1.5 to 1.6 range are compatible with sodium chloride and ammonium sulphate {Seinfeld, 2006 #473}, as well as most mineral dusts {McConnell, 2010 #493}. The range is very close to values for the real part of the refractive index of organic carbon but below the values for black carbon {Kim, 2015 #494}. As a consequence, the refractive index choice might not be accurate for a black carbon dominated sample. However, black carbon is highly unlikely to dominate in the size range where a value of the real part of the refractive index of 1.7 dramatically changes the size distribution (diameters above 0.5 µm) {Seinfeld, 2006 #473}, so our refractive index choice is valid. In Fig. 5b one can see that changing the imaginary part of the refractive index from 0 to 0.01 only produces small changes in the distribution. The imaginary part of the refractive index of many aerosol types as sodium chloride, sulphates and mineral dust falls within the shown range {Seinfeld, 2006 #473}, {McConnell, 2010 #493}. For values of the imaginary part of the refractive index above 0.01 (not shown in the image), the size distribution dramatically changes for sizes above 1 µm (but not for smaller values of it), overlapping and disagreeing with the CDP. However, values above 0.01 in the imaginary part of the refractive index are only associated with strongly absorbing aerosol like black carbon, which will dominate only in the submicron sizes {Seinfeld, 2006 #473}. The submicron part of the size distribution doesn't change for values of the imaginary part of the refractive index above 0.01, so our refractive index choice is still acceptable even for samples with significant contributions from black carbon in submicron sizes.

Deleted: can only happen in

For the PCASP-CDP, we have considered two uncertainty sources. The first one is the Poisson counting uncertainty in the number of particles in each bin and the second one is the uncertainty in the bin width that is given by the applied optical property corrections. Both sources have been propagated in order to obtain the errors of d*N*/dlog*D*p and d*A*/dlog*D*p. The errors in the bin centre position were given by the calibration. In order to avoid the problems with the transition in between different gain

stages in the PCASP, some bins were merged or eliminated (5 and 6 as well as 15 and 16 were merged, while the bin 30 was eliminated), as indicated by {Rosenberg, 2012 #456@@author-year}. Other uncertainties such as the refractive index assumption or particle shape effect, as well as the uncertainty in the bin position haven't been regarded in this study. Sampling biases haven't been quantified or corrected yet so they haven't been included. The size distributions produced by the PCASP-CDP have been taken as a reference value for the purposes of this study.

4. Scanning Electron Microscopy technique for aerosol characterization

Scanning Electron Microscopy is used in order to study composition and morphology of aerosol particles, in a similar way to previous works such as {Krejci, 2005 #316@@author-year}, {Kandler, 2007 #443@@author-year}, {Chou, 2008 #447@@author-year}, {Kandler, 2011 #442@@author-year}, {Young, 2016 #75@@author-year}, {Price, 2018 #450@@author-year} and {Ryder, 2018 #541@@author-year}. We use a Tescan VEGA3 XM scanning electron microscope (SEM) fitted with an X-max 150 SDD Energy-Dispersive X-ray Spectroscopy (EDS) system controlled by an Aztec 3.3 software by Oxford Instruments, at the Leeds Electron Microscopy and Spectroscopy Centre (LEMAS) at the University of Leeds. In order to get data from thousands of particles in an efficient way, data collection was controlled by the AztecFeature software expansion.

Aerosol particles were collected with the filter inlet of the FAAM aircraft on polycarbonate track etched filters with 0.4 µm pores (Whatman, Nucleopore). Samples for SEM are usually coated with conductive materials in order to prevent the accumulation of charging on the sample surface {Egerton, 2005 #426}. For aerosol studies, materials like gold {Hand, 2010 #444}, platinum {Chou, 2008 #447}, or evaporated carbon {Reid, 2003 #445;Krejci, 2005 #316;Young, 2016 #75} have been used. When it comes to choosing which signal to detect, some previous studies used mainly backscattered electrons {Reid, 2003 #445}{Kandler, 2007 #443}{Gao, 2007 #451}{Kandler, 2011 #442}{Young, 2016 #75;Price, 2018 #450}{Kandler, 2018 #602} and some others choose secondary electrons {Krejci, 2004 #316}{Hamacher-Barth, 2013 #500}. We started the development of this analysis using a carbon coating and the backscattered electron detector. This technique produced reproducible images and almost no artefacts from the pore edges, consistent with {Gao, 2007 #451@@author-year}. However, we noticed that we sometimes undercounted a significant fraction of the small carbon based particles (this strongly depended on the sample), which looked transparent under the backscattered electron imaging but not under the secondary electron detector, as seen in Fig. 6. This likely happened because the contrast in the secondary electron images mainly depends on the topography of the sample whereas the contrast in the backscattered electron images depends on the mean atomic number of each sample phase {Egerton, 2005 #426}. Since the polycarbonate filters are made of C and O, particles containing only these elements in a similar proportion to the background did not exhibit a high contrast under the backscattered electron detector {Laskin, 2001 #439}. However, when using secondary electron imaging with carbon coatings, images were less reproducible and contained artefacts from the pore edges, probably resulting from charging or topographical effects. We found that coating the samples with 30 nm of iridium helps to improve the secondary electron image reproducibility and reduced the pore edge artefacts as well as allowing us to locate small organic particles. An increase in the size of the particle as a consequence of the coating may introduce an uncertainty in the size of the smallest particles. An additional advantage of using Ir is that the energy dispersive X-ray spectrum of Ir does not overlap greatly with the elements of interest.

In the SEM the sample was positioned at a working distance of 15 mm. The SEM's electron beam had an accelerating voltage of 20 KeV and a spot size chosen to produce the optimum number of input

Deleted: and

Deleted: were

Deleted: ing

Deleted: wasn't quantified and

Deleted: s

Deleted: type

counts in the EDS detector. Images are taken at two different magnifications with a pixel dwell time of 10 µs and a resolution of 1024 x 960 pixels per image. High magnification images (40 nm per pixel or smaller) were used to identify particles down to 0.3 or 0.2 µm depending on the sample, and medium magnification images (about 140 nm per pixel) are used to identify particles down to 1 µm. A brightness threshold with upper and lower limits that correspond to pixels of certain shades of grey was manually adjusted for each image by the operator to discriminate particles from the background. Based on the manually set brightness threshold, AztecFeature identified the pixels that fall within the limits as aerosol particles and calculated several morphological properties of the particle as cross sectional area, length, perimeter, aspect ratio, shape factor or equivalent circular diameter. The equivalent circular diameter is defined as $\sqrt{(4\ A\ \pi^{-1})}$, where A the cross sectional area of the aerosol particle. This equivalent circular diameter has not been corrected or transformed into an optical or other equivalent diameter.

For this analysis we placed a section of the 47 mm filter on a 25 mm stub. In order to collect morphological and chemical information from a few thousand particles, we only scanned a fraction of the filter (typically up to 1% of the filter at low magnification and up to 0.01% for high magnification). We collected information from 5 to 20 different areas, and each area consisted of a montage of several SEM images. In Fig. 7 one can see the radial distribution of aerosol particles on top of a filter collected using the inlet system. In spite of some fluctuations (which are up to a factor 3 and appear to be random), one can see that the particles are homogenously distributed all over the central ~30 mm of the filter. As a consequence, the areas were chosen by the user from all over the surface of the selected fraction of the filter. Each area was selected in the software, manually adjusting the particle detection threshold. The Z position of the stage was also adjusted manually for each image in order to produce properly focused images. After doing this, the image scanning and EDS acquisition was performed in an automated way. Morphological information was recorded for all particles with an equivalent circular diameter greater than the specified size threshold (typically 0.2 or 0.3 µm).

EDS analysis was restricted to the first 12 or 15 particles detected in each image. This reduces the likelihood of image defocusing over the SEM automated run. The software performed EDS in the centre of the particles, obtaining around 50,000 counts per particle. The raw data for any given particle were matrix corrected and normalised by the AZtec software to produce element weight percent values with a sum total of 100%, using a value of the confidence interval of 2 (a further discussion on the confidence interval can be seen in the Appendix C). Then particles were categorised based on their chemical composition using a classification scheme which can be created and modified within the AztecFeature software. The characteristic X-rays taken at one point are emitted by a certain interaction volume which is bigger than some of the analysed particles (typically < 2 μm^3, decreasing with atomic number and increasing with incident electron energy). As a consequence, a part of the X-ray counts attributed to each particle come from the background (C and O from the polycarbonate filter and Ir from the coating) and the weight percentages obtained from the X-ray spectra do not match the actual weight percentages of the particle itself. As a consequence, when categorising the particles based on their composition, we only use the presence or absence of certain elements, and the ratio between the weight percentages of non-background elements. The classification scheme works by checking if the composition of each particle falls within a range of values which are manually defined by the user. Particles not matching the first set of rules are tested again for a second set of rules, and so on, until reaching the last set of rules. A few sets of rules can be merged into a category. In the supplementary information (Fig. S3), we give the details of the 32 sets of rules used, which are then summarised into 10 composition categories. A description of the most abundant elements in each category and an interpretation of these categories is included in Appendix B.

Deleted: x 5000 or similar

Deleted: x1500 or similar

Deleted: ’

Deleted: don’t seem

Deleted: to be

Deleted: adial

Deleted: The areas were chosen by the user from all over the surface of the selected fraction of the filter, since aerosol particles were evenly distributed all over the central ~30mm of the filter (the area which exposed to the air) as one can see in Fig. 7.

Deleted: charging problems caused by exposure to the electron beam.

Deleted: Fig. S1

Deleted: Sect. 5

The detection of particles has certain limitations. The edges of the pores can look brighter than the rest of the filter in the SE images (probably because they consist of a larger surface area from which secondary electrons can be generated, hence a larger signal). As a consequence, they can look like ~0.2 µm particles, which is the main reason why particles below 0.3-0.2 µm (depending on the sample) are not included in this analysis. These artefacts had a chemical composition similar to the filter, so they were labelled as "Carbonaceous" by the classification scheme, falling at the same category as most biogenic and black carbon particles. However, these artefacts were only around 1 to 10 percent depending on the sample. If they appear in larger quantities, they can be removed manually after or during the analysis. Another limitation arises from the fact that some aerosol particles did not have sufficient brightness in the SE image and were not detected as a particle. This happens more frequently for submicron particles (especially the ones closer to the limit of detection), but it can also happen with some coarse mode aerosol particles, particularly if they are only composed of Na and Cl or S. This issue can be addressed if necessary by setting a very low limit of detection, which adds lots of artefacts as well as the low brightness particles, and then removing the artefacts manually (the artefacts can be easily identified by the user). In other infrequent instances, only a fraction of the particle had a brightness above the threshold, so they were detected as a smaller particle or multiple smaller particles, or if two particles are close enough, they can be detected as a single larger particle. However, we feel that in the vast majority of the cases a representative cross sectional area of the particle was picked by the software.

Blank polycarbonate filters can contain some particles on them from manufacturing or transport before being exposed to the air. In addition, handling and preparing the filters can introduce additional particles to it. In order to assess these artefacts, we scanned a few clean blank filters. We also examined a filter that had been brought to the flight, loaded in the inlet system (but not exposed to a flow of air), and then stored at -18 °C for a few months (like most of the aerosol samples on filters). The results of both the handling blank and the blank can be seen in Fig. S2. The number of particles is typically about the order of magnitude of one particle per 100 by 100 µm square, which is more than an order of magnitude below all the samples in this study (apart from the sample shown in Fig 9c which was taken in a very low aerosol environment, where it is only about a factor 2). In Fig. S2 one can see that about half of particles found in both blank filters and the handling blank belong to the metal rich category. However, further examination of the composition of these metal rich particles revealed that almost all of them were Cr rich particles (about 97 % in the case of the blank filters and about 96% in the case of the handling blank). As a consequence, we excluded all the Cr rich particles from the analysis of atmospheric aerosol. By doing this, we make sure that we exclude about half of the artefacts of the analysis. There was a contribution of mineral dust origin particles (Al-Si rich, SI rich and Si only) for sizes in between 0.7 and 5 µm in the handling blank (less than 10% of the number in the handling blanks). Generally, the composition of the particles present in the blank filters and in the handling blank was very similar, suggesting that most of these artefacts are not produced by the loading, manipulation and storage of the filter.

Deleted: Size distribution of the background aerosol particles that one can find in the blank or handling blank hasn't been shown, and it needs to be compared with each individual sample individually.

Deleted: very low,

Deleted: well below the typical particle loading on a filter exposed to the atmosphere

Deleted: the vast majority

Deleted: lic

Deleted: these

Deleted: (it was only ever a very minor component).

Deleted: T

Deleted: However, there was a very small but significant contribution of mineral dust origin particles (Al-Si rich, SI rich and Si only) for sizes in between 0.7 and 5 µm in the handling blank, which should be taken into consideration.

5. Inlet characterisation and sampling efficiency using Scanning Electron Microscopy

In order to experimentally test the inlet efficiency, to complement the efficiency calculations presented in Section 2.2, we have used SEM to quantify the size distribution of particles collected on filters (Sect. 4) and compare this with the measurements from the under-wing optical probes (Sect. 3). The calculations in Sect. 2.2 suggest that there is an enhancement of the coarse mode aerosol particles, which is larger when sampling with the bypass closed. To test this we have collected aerosol onto 0.4 µm pore size polycarbonate filter in both lines in parallel and show these results in Fig. 8. In

one of the lines, the bypass was kept open, and in other line the bypass was kept closed. Using our SEM approach described in the Sect. 4, we calculated the size distribution of the aerosol particles on top of each filter. We compared these size distributions with the ones measured by the underwing optical probes (PCASP-CDP), as described in Sect. 3. We performed the comparison twice in two different test flights based in the UK.

One can see that the concentration of aerosol particles measured by the SEM on the filters was higher than the particles detected by the optical probes for sizes above ~8 µm in Fig. 8 (reaching about an order of magnitude in number around 10 µm in both cases). These results are consistent with {Price, 2018 #450@@author-year} and {Ryder, 2018 #541@@author-year}, where they observed an enhancement of coarse aerosol particles in mineral dust dominated samples collected close to Cape Verde. In addition, the enhancement was larger when sampling with the bypass closed (about a factor 2-3). The results of these comparisons are in qualitative agreement with the theoretical calculations in Sect. 2.2, i.e. that the sub-isokinetic enhancement is reduced with the bypass open.

After establishing that having the bypass open produces a more representative sampling of coarse mode aerosol we then had the bypass open for the subsequent sampling. In Fig. 9 we have presented some other bypass open SEM size distributions compared with the PCASP-CDP data from three different aerosol samples in contrasting locations. Since these data were taken during the scientific field campaigns and not test flights, we only collected one polycarbonate filter for SEM since the other line was used for INPs analysis on Teflon filters (not shown here). In Fig 9a, one can see a sample collected in the UK where there is an enhancement of the coarse mode which reaches almost an order of magnitude at 10 µm. The sample shown in Fig 9b was collected in Iceland, and the enhancement of coarse aerosols can be seen through most of its range, reaching even the first two bins of the submicron aerosol range. In Fig 9c one can see a sample collected in North Alaska where the coarse mode aerosol concentration was one to two orders lower than the examples from the UK and Iceland. In this case the SEM size distribution is only about a factor 2 above the size distribution of the handling blank, nevertheless the SEM and optical probes both produce similarly low numbers of coarse mode aerosol. The low number concentration results in the lack of data in the SEM above 7 µm and the large uncertainties in the PCASP-CDP above 1.5 µm. We do not observe a coarse mode enhancement in this sample, probably because of the low aerosol concentration in the size range where we expect the largest biases and large uncertainties.

In the submicron range, one can see that in all the comparisons shown in Fig. 8 and Fig. 9 there is sometimes an undercounting in the SEM size distribution when compared with the optical probes. Generally, the undercounting increases with decreasing size and reaches an order of magnitude or more, as one can see in Fig. 8, Fig. 9a and Fig. 9c; this is qualitatively similar to {Young, 2016 #75@@author-year}. There are several potential reasons for this. We can rule out particles simply being lost by passing through the 0.4 µm polycarbonate filters, since they are known have a high collection efficiency {Lindsley, 2016 #415;Soo, 2016 #462}, although some of them might deposit inside the pores and therefore not be detected. In addition, it is likely that some small particles are not sufficiently bright to be detected, despite the fact we made efforts to mitigate this problem with the use of secondary electrons and the Ir coating (see figure 6). Also, volatilization of certain types of aerosol particles (which are more abundant in the submicron fraction {Seinfeld, 2006 #473}) can occur during heating (in this case produced by deceleration of the flow in the inlet) or sampling {Bergin, 1997 #537;Nessler, 2003 #538;Hyuk Kim, 2015 #531} and this effect could be enhanced by the fact that

Deleted: Some of the shown PCASP size distributions present some bumps (particularly above 2 µm), but it is not possible to address if they are physical or just an artefact produced by the calibration {Rosenberg, 2012 #456}. Given the uncertainties on both techniques and the fact that they measure different diameters (optical diameter in the case of the PCASP-CDP and geometric equivalent circular diameter in the case of the SEM), this comparisons cannot be used to exactly quantify the biases on the system but understand its presence. For similar reasons, the SEM data hasn't been corrected using the theoretical efficiency. ¶
The results of these comparisons can be seen in Fig. 88 and Fig. 9 for both number and surface area size distribution. There are some discrepancies between the optical probes and the SEM size distributions from the filters, which has also been reported in previous works {Chou, 2008 #447}, {Young, 2016 #75;Price, 2018 #450}{Ryder, 2018 #541}. The SEM detected less submicron aerosol particles on the filter

Deleted: 8 and Fig. 9

Deleted: For the case shown in Fig 8b, it seems that the optical probes measured the same amount of aerosol abo

Deleted: a similar

Deleted: two

Deleted: under

Deleted: bypass

Deleted: conditions

Deleted: suggest that the filter inlet system has the same type of bias for coarse aerosol particles as theoretically

Deleted: again undercounting of submicron particles (even tough in this case it only happens for sizes bellow 400 nm)

Deleted: Some undercounting of submicron aerosol can be seen below 500 nm.

Deleted: In this case, both the optical probes and the SEM detected a very low amount of coarse aerosol particles

Deleted: counting

Deleted:)

Deleted: This comparison does n'ot allow us to see any coarse mode enhancement because of the low coarse

Deleted:), but one can see again the increasing undercounting of submicron aerosol particles (reaching an

Deleted: Overall,

Deleted: d

Deleted: of the submicron aerosol particles

Deleted: The

Deleted: for the second comparison as one can see in Fig. 8b

Deleted: very

Deleted: Instead

Deleted: happen

samples are exposed to high vacuum during the SEM analysis. In addition, the SEM techniques measure the dry diameter and the optical probes measure the aerosol diameter at ambient humidity. This hygroscopic effect shifts the dry size distributions to smaller sizes, which might also explain part of the disagreement {Nessler, 2003 #538;Young, 2016 #75}. Disagreement in the measurements can also be produced by the fact that the techniques are measuring different diameters (optical and geometric).

Some of the PCASP size distributions contain some 'bumps' (particularly above 2 µm), but it is not possible to address if they are physical or just an artefact produced by the refractive index correction {Rosenberg, 2012 #456}. Given the uncertainties on both techniques and the fact that they measure different diameters (optical diameter in the case of the PCASP-CDP and geometric equivalent circular diameter in the case of the SEM), this comparisons cannot be used to quantify the biases in the system, but can be used to make a qualitative comparison. For similar reasons, the SEM data has not been corrected using the theoretical efficiency.

6. Application to samples collected from the atmosphere above S.E. England and North Alaska

The SEM technique to produce size resolved composition of aerosol samples described in Sect. 4 has been applied to samples collected from the FAAM aircraft in various locations. In Fig. 10 we show an example of some of the capabilities of this technique applied to a sample collected in S. E. England. The purpose of this section is purely to give examples of the capabilities of the technique, further analysis is planned for subsequent papers. The fraction of particles corresponding to each compositional category described in Appendix B for each size can be seen in Fig. 10a and the corresponding number size distribution of each composition category can be seen in Fig. 10b. By looking at this analysis, one can see that the sample carbonaceous aerosol particles made a substantial contribution to the number across the full distribution and there was a clear mineral dust mode (Si only, Si rich Al-Si rich and Ca rich) for particles larger than about 1 µm. There was also a smaller contributions of metal rich and S rich aerosol particles, particularly in the fine mode. A potentially useful application of the size resolved composition is calculating the surface area or mass of an individual component of a heterogeneous aerosol. As an example, we have grouped the mineral dust categories Si only, Si rich Al-Si rich and Ca rich to produce the surface area size distribution of mineral dust (and potentially ash) in Fig. 10c.

In Fig. 11 we show six examples of the size-resolved composition of different aerosol samples in two locations (South East England and North Alaska). We can see that the aerosol samples are very different depending on the location. The aerosol samples collected in the UK shown in Fig 11a, c and d are very similar to the sample shown in Fig. 10a. In fact the sample in Figure 10a was taken on the same day in a similar location as the sample in Fig 11b and the similarity between the two helps to demonstrate the reproducibility of our technique. Generally, these samples from S.E. England contained carbonaceous aerosol throughout the size distribution, particularly in the fine mode. This is consistent with typical urban influenced aerosol {Seinfeld, 2006 #473}. There is also a substantial proportion of mineral dust and only a small proportion of Na rich aerosol. In contrast, the samples collected in North Alaska (close or above the Arctic Ocean) generally contained a smaller proportion of carbonaceous particles, but much larger contributions of Na rich aerosol (very likely sea salt particles, since they were collected in a marine environment). The S-rich category was also substantial

Deleted: be

Deleted: is

Deleted: shown

Deleted: present

Deleted: '

Deleted: ¶
¶
In Fig. 10 we have presented some other SEM size distributions compared with the PCASP-CDP data from three different aerosol samples in contrasting locations. Since these data were taken during the scientific field campaigns and not test flights, we only collected one polycarbonate filter for SEM since the other line was used for INPs analysis on Teflon filters. All the sampling was done with the bypass open. The agreement between the optical and SEM obtain...

Moved down [2]: 6. Recommendations for aerosol

Deleted: ¶ ...

Moved down [1]: 7. SEM compositional categories ¶

Deleted: The data shown in this section have been obtain...

Deleted: rules described in the supplementary informatio...

Deleted: a

Deleted: Here

Deleted: developed

Deleted: one of the

Deleted: s

Deleted: ; the resulting size resolved composition is show...

Deleted: an

Deleted: so no further scientific analysis has been include...

Deleted: Sect. 7

Deleted: . The

Deleted: SEM

Deleted: was clearly dominated by

Deleted: in all the sizes, but

Deleted: and some

Deleted: other aerosol types (

Deleted:)

Deleted: There are very few ways to obtain the size-...

Deleted: 6

Deleted: o

Deleted: (Seinfeld and Pandis, 20)

Deleted: , which was previously described (the latter and...

Deleted: exhibited much less

Deleted: taken

in the fine mode in Alaska, consistent with some samples collected in other areas of the Arctic {Young, 2016 #75}, and some samples collected in a similar location {Creamean, 2018 #604}. Notably, the coarse mode in Alaska, while generally smaller in number than in S.E. England, contained a high proportion of mineral dusts. This is also consistent with other measurements in the Arctic {Young, 2016 #75}{Creamean, 2018 #604}.

6. Recommendations for aerosol sampling with the Filters system on the FAAM aircraft

Based on the calculations in Sect. 2.1 and the experimental findings in the subsequent sections, we suggest keeping the total flow rate (including the flow through the filters measured by the electronics box plus the bypass flow, which can be between 20 and 35 L min^{-1}) above 50 L min^{-1}. Below this range, the sub-isokinetic enhancement of large aerosol particles is above a factor 2, according to the calculations in Sect. 2.2 that can be seen in Fig. 2b. For total flow rates above 65 L min^{-1}, the flow becomes turbulent throughout the line, which associated losses. However, the calculations shown in Fig. 2c indicate that the combination of the isokinetic enhancements and turbulent losses at 80 L min^{-1} lead to a reasonably representative sampling, but when it reaches 150 L min^{-1}, the position of the D50 drops to 6.5 µm (not shown in the graph) so such a high flow rate would not be appropriate if the user wants to sample coarse aerosol particles. Hence, we recommend an operational upper limit of 80 L min^{-1}. For 0.45 µm PTFE filters and the 0.4 µm polycarbonate filters presented in Fig. 4, sampling close to this flow rate range is often achievable by keeping the bypass open, since this increases the total flow rate and brings it closer to the suggested range, as one can see in Fig. 2c. If other filter types are used, the flow rates will be different to those presented here and these flow rates should be taken in consideration when choosing the pore size (or equivalent pore size) in order to avoid dramatic sampling biases.

We already mentioned in Sect. 2.3 that we recommend replacing the side displacement pump with a design that would provide a greater pressure drop. In addition, we also recommend that the bypass flow rate is also routinely measured and controlled in order that the flow at the inlet nozzle can be optimised while sampling.

9. Conclusions

In this work we have characterised the filter inlet system on board the FAAM BAe-146 research aircraft which is used for the collection of atmospheric aerosol particles for off line analysis. Our primary goal is to use this inlet system for quantification of INP concentrations and size resolved composition measurements, but it could also be used to derive other quantities with other analytical techniques.

In order to characterise the inlet system we made use of an electron microscope technique to study the inlet efficiency, by comparing the SEM size distributions with the in situ size distributions measured with underwing optical probes (PCASP-CDP). In spite of the discrepancies and uncertainties, the sub-isokinetic enhancement of large aerosol particles predicted by the calculations in Sect. 2.2 was observed in these comparisons. We also experimentally verify that this enhancement is minimised by operating the inlet with the bypass open which maximised the flow rate through the inlet nozzle. In addition, we note that we performed tests with three very different aerosol distributions and the size distribution of the particles on the filters had comparable features and concentrations to those measured by the underwing optical probes. Overall, the inlet tends to enhance the concentration of aerosol in the coarse mode with a peak enhancement at ~10 µm, but when operated with the

Deleted: , and sulphates,

Moved (insertion) [2]

Deleted: ideal

Deleted: se results should

Deleted: The

Deleted: was

recommended flow conditions this enhancement is minimised. The inlet efficiency decreases rapidly for sizes above about 20 µm and becomes highly dependent upon the specifics of the sampling such as flow rates and angle of attack. Based on the calculations we recommend that the total flow rates at the nozzle are maintained at between 50 and 80 l min^{-1}, and also that improvements are made to the pump and bypass flow control (see Sect. 2.3).

We also established an SEM technique to determine the size resolved composition of the aerosol sample. Each particle can be categorized based on its chemical composition using a custom made classification scheme. Using this technique we showed that the filter system on board of the FAAM BAe-146 spreads the particles evenly across the filter surface, which is necessary for the SEM size distribution analysis.

Having a well characterised inlet allows us to sample aerosol particles up to around 20 µm with knowledge of the likely biases from the aircraft. Hence, we can use this inlet system to collect aerosol for offline analysis at altitudes which are relevant for clouds. For example, this may allow us to use the size resolved aerosol composition to quantify the size distribution of individual aerosol components at a particular location and combine this information with INP measurements to quantify the surface area normalised ice nucleating ability of a specific class of aerosol.

Deleted: to with about a factor of 2.

Deleted: se

Deleted: tests

Appendix A: discussion of the inlet efficiency calculations

Here we include a further description of the efficiency mechanisms used in the inlet model described in Fig. 2 and discuss the choice of the equations and their limits of validity:

Aspiration efficiency accounts for the fact that the speed of the sampled air mass (U_0), and the speed of the air through the beginning of the nozzle (U) are different. When these two speeds are equal, the sampling is called "isokinetic", whereas when the speeds don't match, the sampling is called super isokinetic or sub-isokinetic depending on if U_0 is smaller or larger than U respectively. In our case, the air mass moves at the flying speed, which varies with the altitude (110 m s^{-1} is a typical value for sampling altitudes), and the speed at the start of the inlet is almost always below 35 m s^{-1} (sub-isokinetic conditions). As a consequence, some air streamlines will be forced around the inlet, while high inertia particles won't, which will lead to an aspiration efficiency above 1 for coarse mode aerosol particles. This enhancement is greater for large particles due to their large inertia which makes difficult their ability to follow the air streamlines. The enhancement reaches a maximum value of U_0/U in its high diameter limit (when none of the particles in the sampled air mass follow the streamlines that escape from the inlet and all of them are sampled). The aspiration efficiency tends to 1 (no enhancement) for small diameters.

This behaviour has been characterised by several studies (we will only look at the sub-isokinetic range of the equations since it is impossible to reach the super isokinetic range during flight). An empirical equation was developed based on laboratory experiment by {Belyaev, 1972 #499@@author-year} and {Belyaev, 1974 #498@@author-year} (referred as B&L) for certain range of U/U_0 ratio and Stokes number. However, for ratios below its experimental range (U/U_0>0.2), the B&L function doesn't make physical sense since it converges to values above 1 for small particle sizes. The aircraft inlet system works at smaller U/U_0 ratios sometimes, so this function is not very accurate to describe the behaviour of the system in such conditions. {Liu, 1989 #458@@author-year} developed another function (referred as LZK) by means of a numerical simulation based on computational fluid mechanics. The U/U_0 ratio and Stokes number valid range is wider than the B&L expression (down to 0.1). It agrees with the B&L expression in the U/U_0 ratio the latter was developed for. For smaller values of the ratio, the LZK function are believed to be more accurate, since it predicts the known physical behaviour (no sub-isokinetic enhancement for small particle sizes). It reaches U/U_0 ratios down to 0.2, which is enough to cover most of the total flow rates achieved in the inlet system. {Krämer, 2004 #459} developed another expression (referred as K&A) for 0.007< U/U_0<0.2 based on computational fluid dynamics. However, for low particle sizes, the efficiency doesn't converge to 1. As a consequence, we have used the LZK {Liu, 1989 #458} function since it covers most of the U/U_0 ratios we get in the inlet system, it agrees with the experimental data in {Belyaev, 1972 #499@@author-year} and {Belyaev, 1974 #498@@author-year} and it converges to U_0/U for large particles sizes and 1 for small particle sizes. Outside its valid range ($U/U_0 < 0.1$), the LZK function agrees with the K&A function for large radius and converges to 1 for small particle sizes. The equation is valid for 0.01<Stks<100, which is enough to cover the range in between 1 and 100 µm. As already stated, it tends to 1 for small particles sizes and to U_0/U for large particles sizes (At 50 L min^{-1}, the ratio U/U_0 is 0.2). All the calculations were done under standard conditions (0 °C and 1 bar). The effect of changes in pressure and temperature (and therefore air density and dynamic viscosity) that normally occur in the filter inlet system sampling range (0 to 3000 m), are negligible in all the used equations

The used equations (as well as the ones used for anisoaxial losses) have been developed for thin-walled nozzles, (this criteria was defined first in {Belyaev, 1974 #498@@author-year}). The inlet has been described as thin-walled in the literature {Talbot, 1990 #453}{Andreae, 2000 #294}{Formenti, 2003 #271} but we haven't used this terminology here since it is not possible to numerically quantify

this using the criteria given in {Belyaev, 1974 #498} because the edge of the nozzle is curved. However, the inlet has been designed to avoid distortion of the pressure field at the nozzle tip and the resulting problems associated with flow separation and turbulence {Andreae, 1988 #296} which is the main caveat of inlet nozzles that are not thin-walled {Belyaev, 1974 #498}. As a consequence, we used these sets of equations for thin-walled nozzles to describe the filter inlet system considered in this study. The fact that the calculations done using this equations show that the filter inlet system has biases with similar characteristics as the ones estimated experimentally for coarse aerosol particles helps to support this assumption.

Deleted: back up

*Inlet inertial deposition i*s defined as the inertial loss of aerosol particles when they enter nozzle. It is produced by the fact that the streamlines bend towards the walls at the moment they enter the nozzle, some large inertia particles can impact the walls and get deposited. Here, we have used the equation given in {Liu, 1989 #458@@author-year} which quantifies this effect. It is also valid for 0.01<Stks<100, which is enough to cover the range in between 1 and 100 µm.

Turbulent inertial deposition happens when some particles are collected by the wall when travelling in a pipe in the turbulent regime because some of the particles cannot follow the eddies of the turbulent flow. In order to include this mechanism, we used the equation given in {Brockmann, 2011 #344@@author-year}, using the relation in between the deposition velocity and dimensionless particle relaxation time given by {Liu, 1974 #461@@author-year}. These calculations are valid for a cylindrical pipe, whereas the turbulent section of the inlet considered here is the nozzle, which has a conical shape. In order to account for this, we divided the conical nozzle into 90 conical sections with an increasing diameter and a length of 1mm, and combined the effect of all the sections. This approach does not account for the additional inertial losses that could occur as a consequence of the enlargement of the flow in the conical section. As already mentioned, above 65 L min^{-1}, turbulent flow occurs in the whole inlet tube. This has been taken into account in the 80 L min^{-1} case in Fig. 2b. The equation used here has been tested for size ranges in between 1.4 and 20 µm, and doesn't depend on the Reynolds number values it was tested for (10000 and 50000) {Liu, 1974 #461}.

Deleted: ’

Bending inertial deposition was also considered, since the line curves with an angle of 45º in order to bring the airstream into the cabin. The inertia of some particles may keep them in their original track and they are not able to follow the air streamlines that are bending towards the cabin, following the inlet tubes. In order to account for these losses, we have used the empirical equation given in {Brockmann, 2011 #344@@author-year} based on the data from {Pui, 1987 #454@@author-year} for laminar flow. This equation was developed for Reynold numbers of 1000, and we have used it for higher values. However, in {Brockmann, 2011 #344@@author-year}, one can see that the data from {Pui, 1987 #454@@author-year} for Re=6000 (beginning of the turbulent flow regime) doesn't differ that much from the fit we have used (valid for Re=1000). Since our Re numbers for the thick section of the tube almost never go above 5000, we can still use the laminar flow fit. This model has been tested for 0.08 < Stks < 1.2, which is enough to cover most of the range where the inertial deposition efficiency drops from 1 to 0. The main caveat of this calculation is that the model considers a smooth tube where that the flow rate before and after the bending is the same, while in the inlet system, if the bypass flow is on, the flow rate before and after the bending is different (before it, it would be equal to the total flow rate, whereas after the bending, it would be equal to the filter flow rate). As a consequence we assumed that the flow rate after the bending is equal to the total flow rate. This assumption might underestimate the losses since some large aerosol particles will become accumulated in the bypass.

Deleted: .

Gravitational settling was also considered. We used the analytical equation given by {Thomas, 1958 #465@@author-year}, as stated in {Brockmann, 2011 #344@@author-year}. We applied this equation

for the section of the pipe from the nozzle to the bend (15 cm long). We used the modification (also analytical) of the previous equation given in {Heyder, 1977 #466@@author-year} in order to account for the losses in the second section of the tube which is 40 cm long and it is bended 45°. The gravitational losses in the nozzle were neglected since the settling distance is much shorter and the time the air takes to pass it is smaller since it travels quicker. As stated previously, the lower part of the turbulent regime can be reached for high flow rates through all the tube. For these cases, we still use this equation which is only valid for the laminar regime, since the gravitational settling efficiencies for the turbulent regime are very close to the laminar regime ones {Brockmann, 2011 #344} and wouldn't make a significant difference in our calculations.

Diffusional efficiency accounts for the fact that small aerosol particles could diffuse to the walls of the pipe via Brownian motion. In order to account for this phenomenon, we have used the analytic equation by {Gormley, 1948 #468@@author-year} as stated in {Brockmann, 2011 #344@@author-year}. We have assumed that diffusion happens only in the tube (before and after the bend) and excluding the diffusion in the nozzle since it is negligible because these losses are a function of the residence time and the residence time of the aerosol particles in the nozzle is much smaller than the rest of the tube. F or this calculation, we have assumed 0 °C and 1 atm. We didn't show the efficiency associated to diffusion in Fig. 2a because it was very close to 1 for all considered sizes. It only becomes slightly smaller than 1 for sizes below 20 nm at 50 L min^{-1}. As a consequence, the inlet could be potentially used to sample nucleation mode aerosol particles, even though for this study we will only focus on the particles larger than 0.1 µm.

Filter collection efficiency accounts for the fact that some particles can pass through the pores of the filter, if they are smaller than the pores. However, filter pore size (in the case of polycarbonate capillarity filters) and filter equivalent pore size (in the case of PTFE porous filters) is sometimes misunderstood as a size cut off at which smaller particles are lost and larger particles are captured. However, particle collection on filters happens through several mechanisms including interception, impaction, diffusion, gravitational settling or by electrostatic attraction under certain conditions {Flagan, 1988 #419;Lee, 1993 #429}. As a consequence, particles with diameters below the pore size are normally collected {Lindsley, 2016 #415;Soo, 2016 #462}. 99.48% of the generated sodium chloride particles with sizes in between 10.4 and 412 nm were collected by a 0.4 µm polycarbonate filter at flow rates below 11.2 L min^{-1} (smaller than most of the flow rates at which the air passes through the same filters in the FAAM filter inlet system) {Soo, 2016 #462}. As a consequence, we assumed a filter collection efficiency of 100% across the whole considered size range (0.1 to 100 µm). However, the fact that some aerosol particles with diameters below the pore size could be deposited in the filter pores and therefore not be detected by the SEM technique could contribute to the undercounting.

Anisoaxial losses have not been considered in the analysis shown in Fig. 2, after estimating that they would only affect particles significantly larger than 10 µm and the fact that the alignment of the inlet is difficult to quantify and the angle of attack changes during the flight. Using the equations explained in {Hangal, 1990 #534@@author-year}, we calculated that the modification of the sub-isokinetic behaviour of the inlet produced by small values of θ is negligible. The equation was used beyond its experimental limit, but this extrapolation was justified by the fact that the equation for θ = 0 made asymptotic physical sense at the low and high Stokes number limits and produced very similar results to the ones showed in Fig. 2a. Anisoaxial sampling can also produce inertial losses when particles impact the walls of the inlet. These ones have been quantified using the expression given by {Hangal, 1990 #535@@author-year} for different values of θ and they can be seen in Fig. 3. This mechanism looks very similar to the gravitational and bend deposition efficiency shown in Fig. 2a. Anisoaxial inertial losses add a cut off that prevents large particles to be sampled. As one can see in Fig. 3, the

effect is very dependent on the angle and only affects particles significantly larger than 10 µm in most cases, so it hasn't been included in the total analysis shown in the Fig 2. One can see in Fig. 3 that the position of the D50 of the anisoaxial cut off decreases when increasing values of θ up to 2°. For values of θ between 2° and 6°, it increases when increasing θ.

Other losses: Some mechanisms (thermophoresis, diffusiophoresis, interception, coagulation and re-entrainment of deposited particles) have not been considered, since they are second order mechanisms under our conditions when compared with the calculated mechanisms {von der Weiden, 2009 #325}{Brockmann, 2011 #344} and for one of them (electrostatic deposition) it is not possible to quantify them. Electrostatic deposition is normally avoided by using grounded conductive materials so no electrical field exists within the tubing {Brockmann, 2011 #344}. Since the FAAM BAe-146 research aircraft is not grounded during the flight, we cannot state this mechanism is irrelevant. However, the experimental agreement between the SEM and optical probes suggest that this is a minor loss mechnanism.

Appendix B. SEM compositional categories

Here we describe the 10 categories we have used in our compositional analysis, which are a summary of the 32 rules described in the supplementary information. The approach has some similarities with the ones in previous studies {Krejci, 2005 #316;Chou, 2008 #447;Kandler, 2011 #442;Hand, 2010 #444;Young, 2016 #75}, but it is distinct. Because of the fact that the filter is made of C and O, background elements (C and O) were detected in all the particles. Particles in each category can contain smaller amounts of other elements apart from the specified ones. This classification scheme has been designed a posteriori to categorise the vast majority of the aerosol particles in the three field campaigns previously described and some ground collected samples in the UK and Barbados. The main limitation of the classification scheme is the difficulty to categorise internally mixed particles. The algorithm has been built in a way it can identify mixtures of mineral dust and sodium chloride (they appear as mineral dust but they could be split into a different category if necessary) and sulphate or nitrate ageing on sodium chloride (they appear as Na rich but it could also be split into a different category). However, other mixtures of aerosol wouldn't be identified, and they would be categorised by the main component in the internal mixture in most cases.

B.1. Carbonaceous

The particles in this category contained only background elements (C and O). The components of the carbonaceous particles consist in either black carbon from combustion processes or organic material, which can be either directly emitted from sources or produced by atmospheric reactions {Seinfeld, 2006 #473}. Particles containing certain amount of K and P in addition to the background elements were also accepted in these category. These elements are consistent with biogenic origin aerosol particles {Artaxo, 1995 #472}. Distinction between organic and black carbon aerosol unfortunately could not reliably be done. Since N is not analysed in our SEM set up, any nitrate aerosol particle would fall into this category if it is on the filter. However, since these particles are semi-volatile, some of these aerosol particles would not resist the low pressure of the SEM chamber. This could be further investigated in the future.

B.2. S rich

Deleted: '

Deleted: es

Deleted: e

Deleted: is mechanism is impossible to quantify because it is not possible to know the distribution of charge in the aerosol particles or the aircraft so it hasn't been included.

Deleted: ¶

Moved (insertion) [1]

Deleted: 7.

Deleted: 7

Deleted: 7

Aerosol particles in this category contained a substantial amount of S. This S might be in the form of inorganic or organic sulphate compounds. Some sulphate compounds, such as sulphuric acid, are relatively volatile and will be lost in the SEM chamber.

Deleted: Aerosol particles in this category contained a substantial amount of S. These EDS signals are compatible with sulphate aerosol particles, which are solid or liquid sulphuric acid particles {Kumar, 2017 #542}. In the same way as the nitrates, this particles are semi-volatile and some of them might not resist the low pressure of the SEM chamber.

B.3 Metal rich

Deleted: 7

The composition of particles in this category is dominated by one of the following metals: Fe, Cu, Pb, Al, Ti, Zn or Mn. These EDS signatures are compatible with metallic oxides or other metal rich particles. These metal containing particles can originate from both natural sources and anthropogenic sources. Some metallic oxides are common crustal materials that could go into the atmosphere but are also produced during some combustion processes {Seinfeld, 2006 #473}. In addition, many types of metal and metallic derivatives particles are produced as component of industrial emissions and other anthropogenic activities {Buckle, 1986 #475}, {Fomba, 2015 #476}.

B.4. Na rich

Deleted: 7

Sodium chloride particles are the main component of the sea spray aerosol particles which are emitted through wave breaking processes {Cochran, 2017 #477}. These particles can age in the atmosphere by reacting with atmospheric components such as sulphuric or nitric acid {Graedel, 1995 #478}, {Seinfeld, 2006 #473}. As a consequence of this reaction, a part of their Cl content will end up in the gaseous phase (as HCl), leading to an apparent chlorine deficit in the aged sea spray aerosol particles. Particles in this category have an EDS signature compatible with sea spray aerosol particles since they are identified by the presence of Na, containing in most cases Cl and/or S (N is not included in our SEM analysis).

B.5 Cl rich

Deleted: 7

Particles in this category contained mainly Cl and sometimes also K but never Na, so they are not sodium chlorine particles. Significant concentrations of Cl and metals in aerosol particles have been linked to industrial activities, coal combustion, incineration and automobile emissions {Paciga, 1975 #480}{Graedel, 1995 #478}, whereas Cl and K in aerosol particles could be originated by the use of fertilisers {Angyal, 2010 #479}, biomass burning {Li, 2003 #501}{Lieke, 2017 #502}, or emitted during pyrotechnic events {Crespo, 2012 #481}.

B.6 Ca rich

Deleted: 7

The composition of the particles in this category is dominated by Ca. In this category, particles containing only Ca (plus C and O, the background elements) are consistent with calcium carbonate, a major component of mineral dust {Gibson, 2006 #482}. If other elements such as Mg and S are present, the signature of the particles compatible with some mineral origin elements as gypsum and dolomite respectively. In addition, presence of minor amounts of Si, Al and other elements could indicate mixing of these Ca rich particles with some other soil components as silicates. However, since Ca is a biogenic element, we cannot discard the biogenic origin of some of the Ca-rich particles {Krejci, 2005 #316}. Some Ca rich particles could originate from the crystallization of sea water, loosely attached to NaCl. The latter component would dominate over the rest of the elements of the conglomerate and they would appear as Na rich particles, unless they shatter in the air {Parungo, 1986 #603}{Andreae, 1986 #503}{Hoornaert, 1996 #504}.

B.7 Al-Si rich

Deleted: 7

Particles in the Al-Si rich category were detected by the presence of Al and Si as major elements. Very often, this particles also contained smaller amounts of Na, Mg, K, Ca, Ti, Mn and Fe. Particles in this category are very likely to have mineral origin and are commonly described as aluminosilicates which include a range of silicates such as feldspars and clays {Chou, 2008 #447;Hand, 2010 #444}. Mixed mineral origin particles containing both Al and Si can also fall into this category. Strong presence of Na and Cl could indicate internal mixing with some sea spray aerosol, whereas a strong S presence could indicate atmospheric acid ageing.

β.8 Si only

The particles in this category contained only Si apart from the background elements. Particles in this category are very likely to be a silica polymorph (mainly quartz), one of the major components of the earth's crust. Since we cannot determine if the C signal in the EDS of these particles is produced from the background or from the particle itself, a particle containing only C, Si and O would fall into this category, however, mineral phases containing these elements are extremely rare.

β.9 Si rich

The composition of these particles was dominated by Si, and other elements Na, Mg, K, Ca, Ti, Mn and Fe. The main difference with the particles in β7 is that the ones described here didn't contain Al above the limit of detection. The EDS signal of particles in this category is compatible with any silicate that does not contain Al as a major component in its phase such as talc or olivine. The only exception is quartz, which falls in the 'Si only' category described above. They could also be internal mixtures of silica or silicates without aluminium as a major component in its phase. Because of the high limit of detection of the Al (See the SI), some particles in this category could contain small amounts of Al, and should belong to Al-Si rich category. As in the Al-Si rich particles case, strong presence of Na and Cl could indicate internal mixing with some sea spray aerosol, whereas a strong S presence could indicate atmospheric acid ageing.

Some of these categories could be further grouped. For example, the particles in the Ca rich, Al-Si rich, Si only and Si rich categories could be considered as "mineral dust". However, if the sample contains ash from combustion processes or volcanic origin, it will also appear in these last categories since its composition is similar to mineral dust {Chen, 2012 #483;Nakagawa, 2003 #486}.

Deleted: 7

Deleted: 7

Deleted: Sect. 7.

Appendix C. Weight percentage confidence level sensitivity test

The software calculates the weight percentage (wt %) of each detected element with its statistical error (σ). In our classification scheme, we have imposed the rule that all the detected elements must be statistically significant in order to be considered as present (the wt % of each detected element needs to be a certain confidence level above the σ. We explored the appropriate value of sigma for our application below.

Our analysis is distinguished from others in the literature in that we use a relatively thick Ir coating (30 nm) as well as a relatively low EDS integration time in order to get data from many particles in a session. Some of the secondary EDS peaks of Ir overlap in some cases with some of the atmospherically relevant elements (the primary peak does not). This produces some issues like a larger σ in some elements. This effect is quite noticeable for Al and S, where some clear peaks of these elements were not statistically significant at a confidence level of 3. In Fig. C1 we show the results of a test where we studied the effect of changing the confidence level from 3 to 2 σ in the particle categorisation carried out by the classification scheme. The only effect of this change yields on the Al and S. When going from 3 to 2 σ as a confidence level, more Al is detected in the sample, so some Si-rich particles (from rule 25) are detected as Al-Si rich particles (rule 5) instead. Manual inspection of a subset of these particles revealed that the Al peak that wasn't being identified at 3 σ is an actual Al signal that was detected at 2 σ. Likewise, some significant S peaks were not being detected at a confidence level of 3 σ but they were at 2 σ, leading to more S rich particles (rule 14) that were labelled as Other from the rule 32 at a higher confidence level. The variation in the confidence level didn't modify the number of particles in other categories, so we recommend the use a 2 σ value in order to minimise the underestimation of Al-Si and S rich particles.

Deleted: to

Deleted: ¶

Acknowledgements

We a grateful for helpful discussions with Paola Formenti (Centre National de la Recherche Scientifique), Hannah Price (FAAM) and Eduardo Morgado (School of Earth and Environment, University of Leeds). Airborne data were obtained using the FAAM BAe-146-301 Atmospheric Research Aircraft, flown by Airtask Ltd and managed by FAAM Airborne Laboratory, jointly operated by UKRI and the University of Leeds. We thank all the people involved in the EMERGE, VANAHEIM and MACSSIMIZE campaigns, as well as Avalon. We acknowledge the Leeds Electron Microscopy and Spectroscopy Centre for the use of their microscopy facilities and the Centre for Environmental Data Analysis for providing us with the FAAM datasets used here. We are grateful for funding from the European Research Council (ERC) (648661 MarineIce).

1312 **References**

1313

Figures

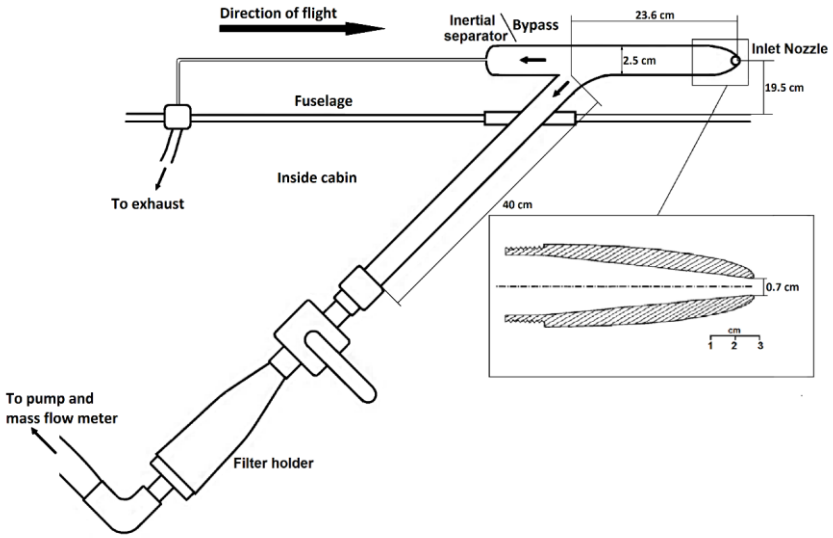

Fig. 1. Schematic diagram of one of the two parallel lines of the Filters inlet system.

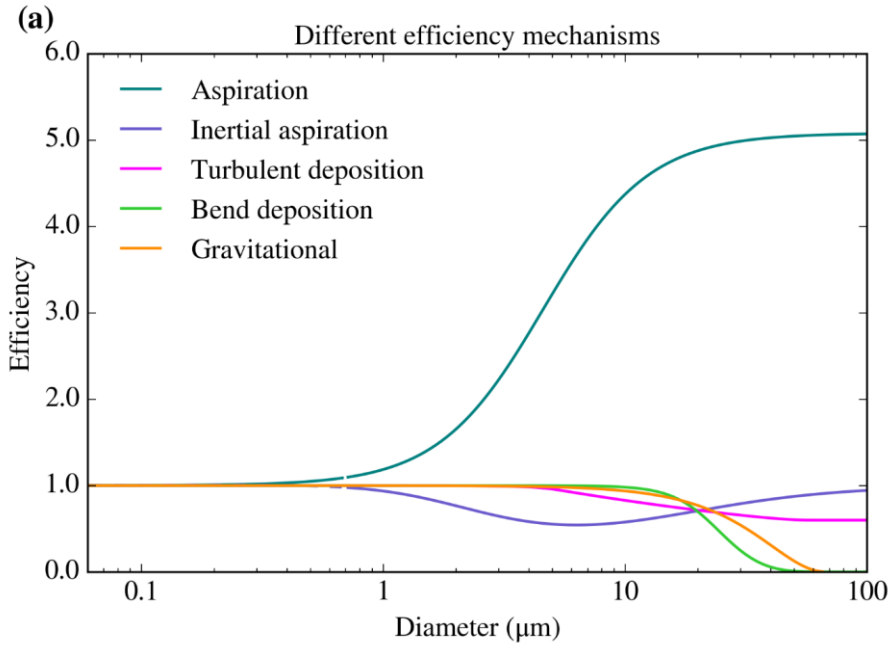
(a)
Different efficiency mechanisms
Aspiration
Inertial aspiration
Turbulent deposition
Bend deposition
Gravitational
Efficiency
6.0
5.0
4.0
3.0
2.0
1.0
0.0
0.1
1
10
100
Diameter (μm)

1317

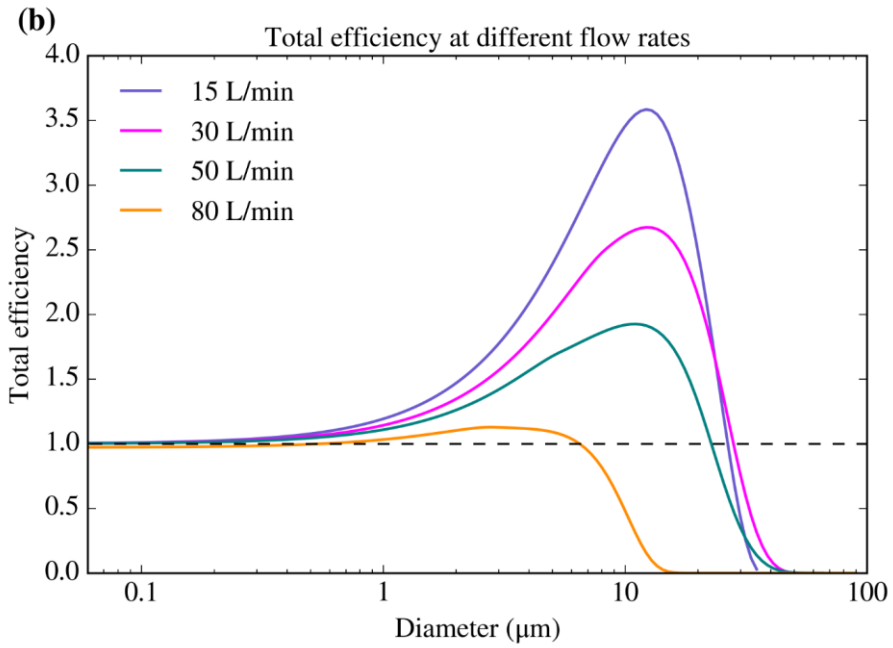
(b)
Total efficiency at different flow rates
15 L/min
30 L/min
50 L/min
80 L/min
Total efficiency
4.0
3.5
3.0
2.5
2.0
1.5
1.0
0.5
0.0
0.1
1
10
100
Diameter (μm)

1318

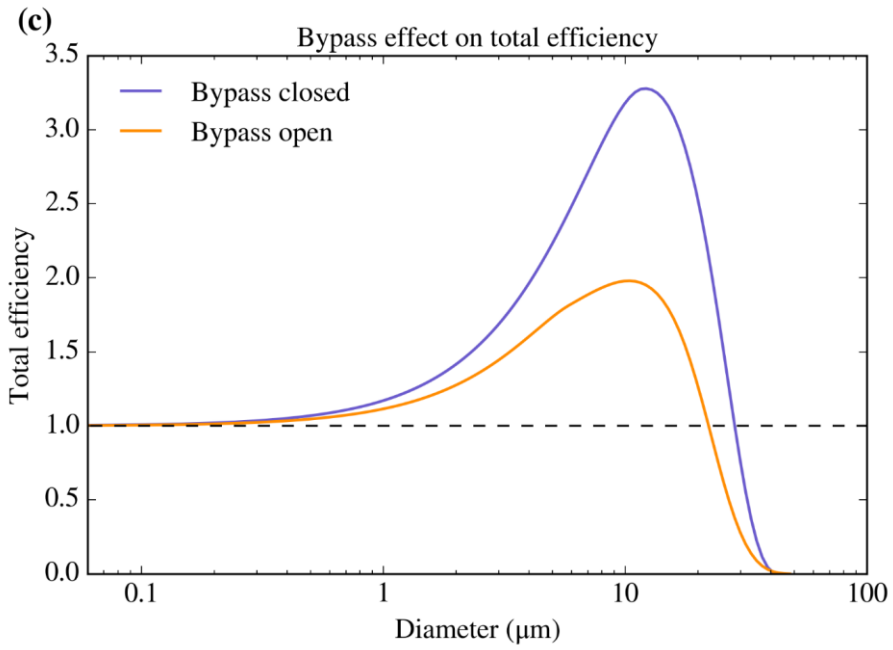

Fig. 2. *Theoretical efficiencies of the Filter inlet system.* (a) Efficiencies of the four mechanisms considered in this work for a total flow rate of 50 L min^{-1}. We have assumed a dynamic viscosity of $1.82x10^{-5}$ kg m^{-1} s^{-1} (value for 0 °C) and a particle density of 1000 kg m^{-3}. The speed of the air mass (U_0) was 110 m s^{-1}, a typical FAAM flying speed at low altitudes. (b) Total efficiency for four different total flow rates. For the 80 L min^{-1} case, turbulent deposition through the whole line was considered since the flow was turbulent through the whole pipe. (c) Total efficiency considering all the described mechanisms for a 20 L min^{-1} filter flow rate with the bypass closed and a 20 L min^{-1} filter flow rate with the bypass open (considering a bypass flow of 25 L min^{-1}).

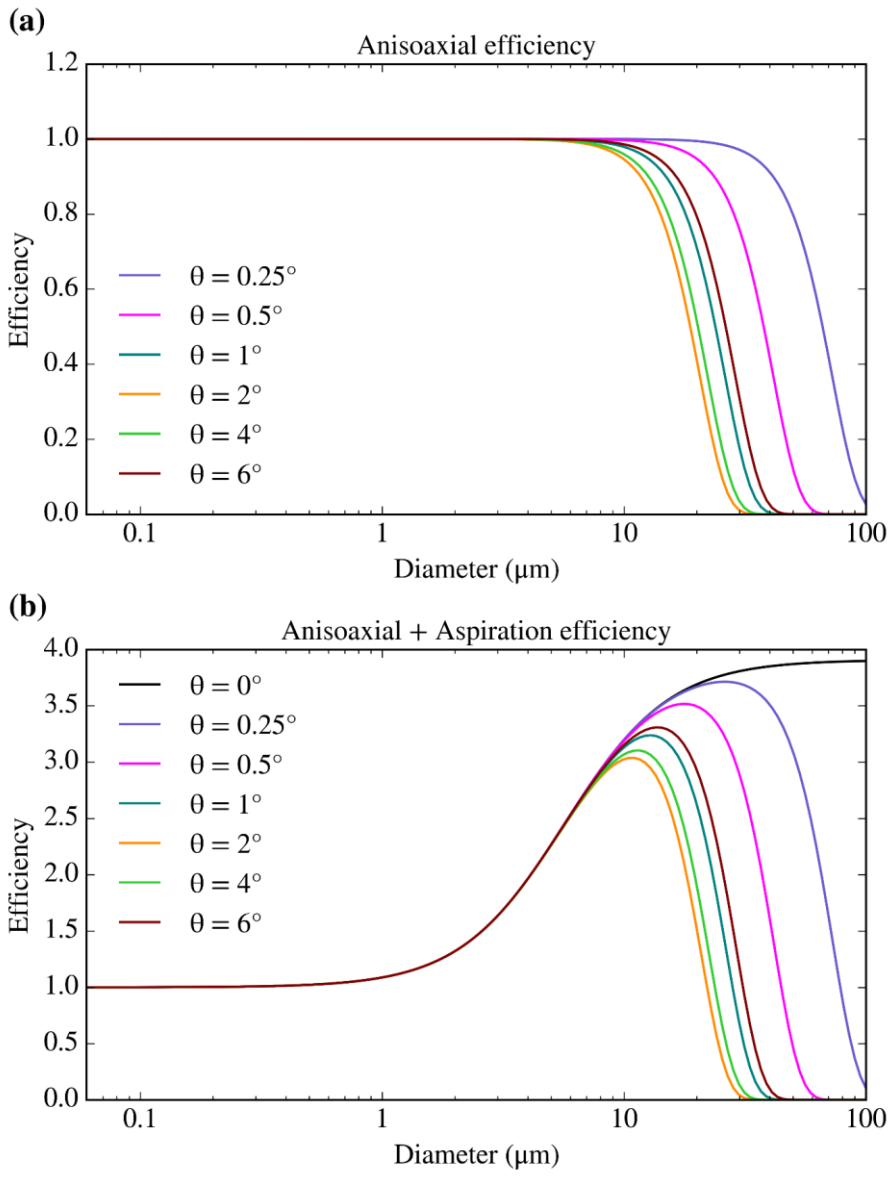

Fig. 3. Anisoaxial inertial losses of the sampling carried out by the Filters inlet system for different values of the angle in between the inlet and the flight direction. The calculations have been presented by themselves (a) and combined with the aspiration efficiency (b), which one can see in Fig. 2a. The anisoaxial calculations have been done using the equations given by {Hangal, 1990 #535}, using the same parameters and dimensions than in Fig. 2, apart from the flow rate, which was set to 65 L min^{-1} in order to be within the valid range of U/U_0 that was used to develop the equation. For smaller or larger values

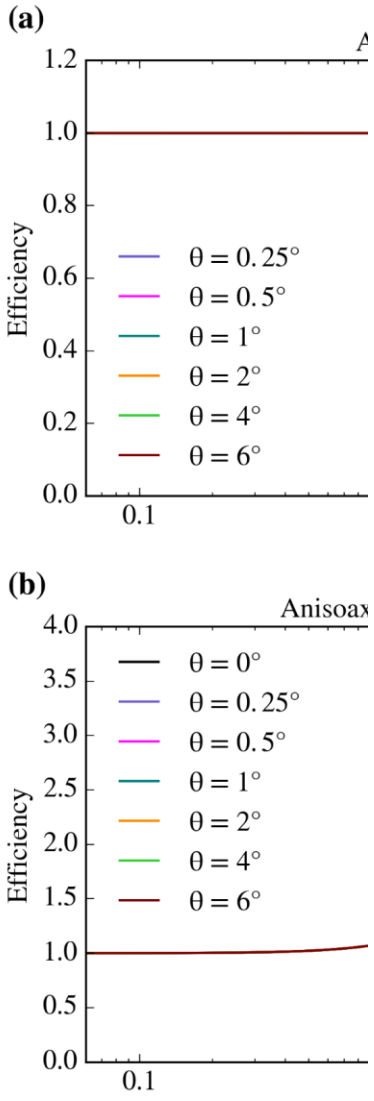

Deleted:

of the flow rate (under which most of the sampling is carried out), the differences in the efficiency from the ones show here are minimal.

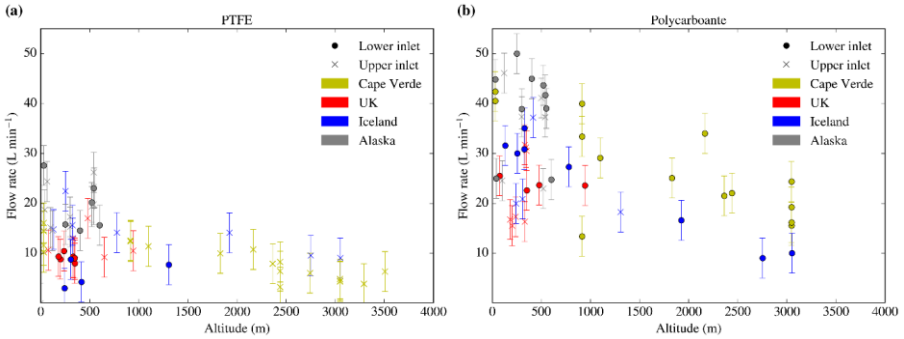

Figure 4. Filter flow rate of different samplings carried out in different campaigns at each altitude using: (a) Sartorius PTFE membrane filters (47mm diameter with a pore size of 0.45µm) and (b) Whatman nucleopore polycarbonate track etched filters (47mm diameter with a pore size of 0.4µm). The crosses represent samples taken in the upper line of the inlet system, whereas dots represent the sampling in the bottom line. Different mesh supports were used for the data collection. The data from Cape Verde was extracted from {Price, 2018 #450} and the notes of the analysis carried out by the authors whereas the altitude data from the other three was obtained from the pressure altitude measurement carried out by the Reduced Vertical Separation Minimum system on board of the aircraft. The altitude data was extracted from the FAAM core datasets C019, C022, C024, C025, C058, C059, C060, C061, C062, C063, C085, C086, C087, C088, C089, C090 and C091 (via the Centre for Environmental Data Analysis). The bypass was closed for all the data in Cape Verde whereas it was open for all the data in the other campaigns. Note that the flow rate here corresponds to the filter flow rate (measured with the mass flow meter), not the total one.

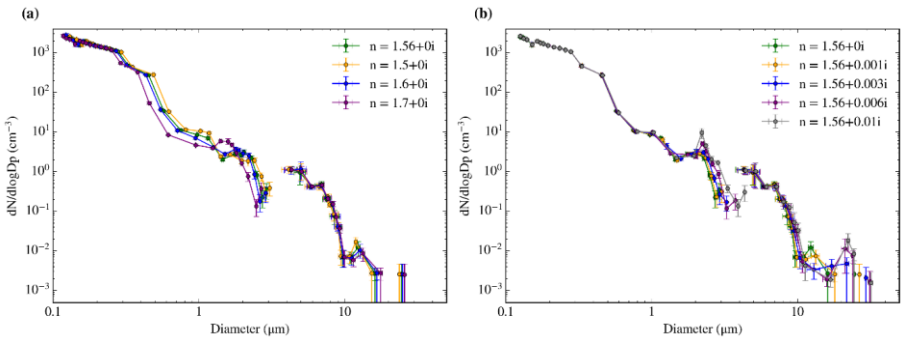

Figure 5. Sensitivity of the size distributions measured by the PCASP-CDP during the C010 flight on the 2017/05/10 from 11:24 to 11:38 UTC to small variations in the refractive index. We tested both the real part (a) and imaginary part (b). The errors are calculated according to the methods explained in Sect. 3.

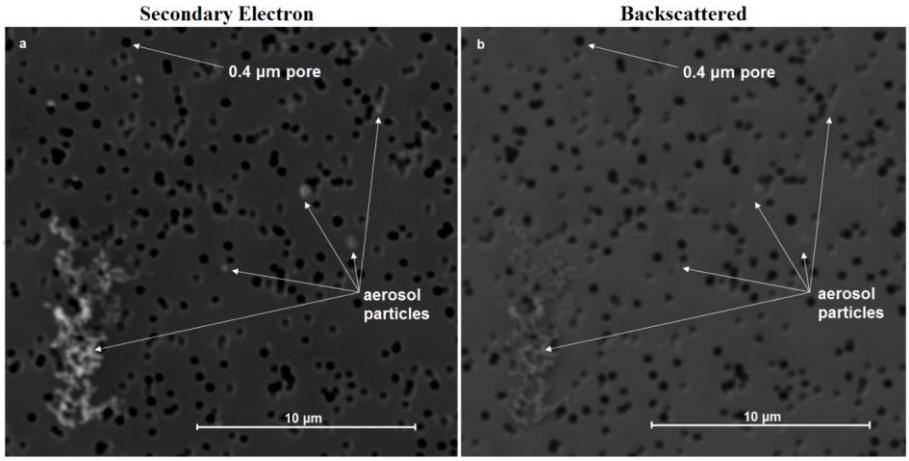

Figure 6. Secondary electron image (a) and Back Scattered Electron image (b) of the same area of the same filter, collected in S.E. England on the 2018/07/05 from 13:32 to 13:47 in the upper line with the bypass open. As one can see, some of the small particles in the SE image appear almost transparent under the BSE image. Even the 10µm soot particle in the bottom left of the image shows a very low contrast in the BSE image.

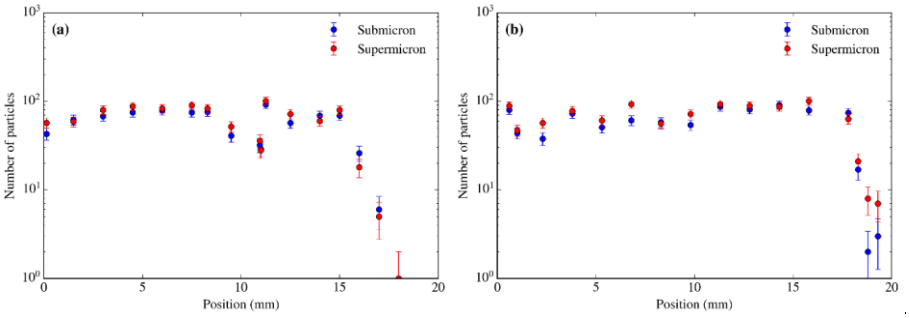

Figure. 7. Radial distribution of particles test on the sample collected on the 2017/10/02 (flight C059) from 16:24 to 16:40 UTC about 320 m high in south Iceland, using the lower line and open bypass, sampling 432 L. Number of submicron and supermicron particles in same size areas (~160x190 μm²) radially distributed versus the distance from the approximate centre through a radius of the filter (a) and another trajectory from the centre of the filter deviated 30º from the first radius (b). The analysis was done at 20 KeV and x5000. The number of both supermicron and submicron particles remains very constant all over the surface of the filter, until reaching the edges of it (which are cover by a rubber O-ring during the sample) and the number of particles drops to the limit of the detection within a few millimetres. The error in the number of particles comes from Poisson counting statistics.

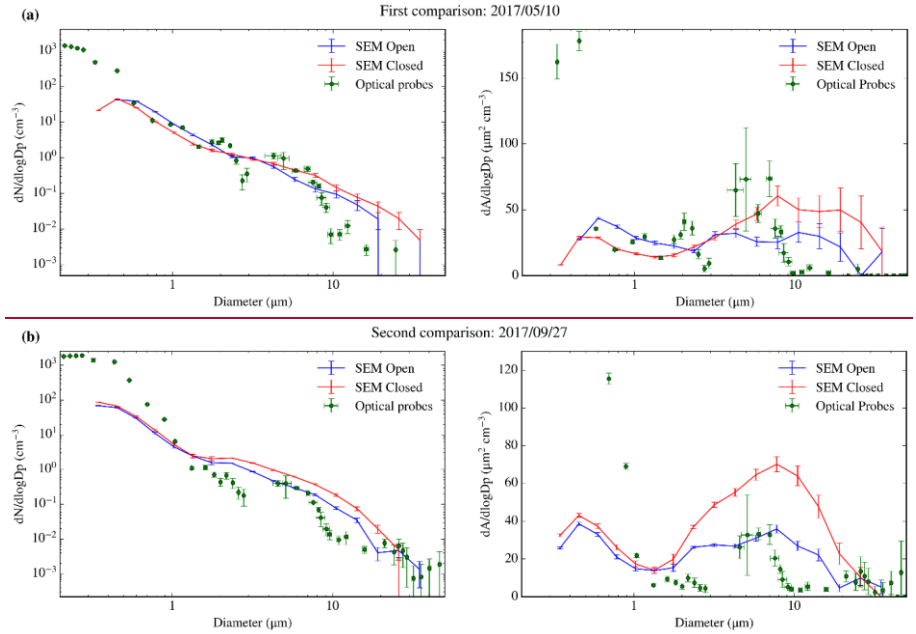

Figure 8. (a) First bypass test carried out during the C010 flight on the 2017/05/10 from 11:24 to 11:38 UTC. The lower line sampled 226 L with the bypass closed, whereas the upper line sampled 141 L with the bypass open at an altitude of about 150 m. The flow rates were 16.1 L min^{-1} and 10.6 L min^{-1} respectively. (b) Second bypass test carried out during the C057 flight on the 2017/09/27 from 13:33 to 13:50 UTC. The lower line sampled 555 L with the bypass open, whereas the upper line sampled 499 L with the bypass closed, at about 240 m. The flow rates were 34.7 L min^{-1} and 31.2 L min^{-1} respectively. The position of the closed and open line was swapped with respect to the first comparison. The sampling was interrupted for a minute to avoid a turn. Both comparisons are shown in both number size distribution and surface area size distribution. The optical probes are the PCASP-CDP, using the closest calibration to the sampling date and a refractive index of 1.56 as stated in the Sect. 2.3. The only error source considered for the SEM size distribution is the Poisson counting error.

Moved down [4]: The optical probes are the PCASP-CDP, using the closest calibration to the sampling date and a refractive index of 1.56 as stated in the Sect. 2.3.

Moved (insertion) [3]

Deleted: B

Deleted: analysis in Fig. 8.

Deleted: The optical probes are the PCASP-CDP, using the closest calibration to the sampling date and a refractive index of 1.56 as stated in the Sect. 2.3.

Moved (insertion) [4]

Moved up [3]: Bypass test carried out during the C057 flight on the 2017/09/27 from 13:33 to 13:50 UTC. The lower line sampled 555 L with the bypass open, whereas the upper line sampled 499 L with the bypass closed. The flow rates were 34.7 L min^{-1} and 31.2 L min^{-1} respectively. The position of the closed and open line was swapped with respect to the first analysis in Fig. 8. The optical probes are the PCASP-CDP, using the closest calibration to the sampling date and a refractive index of 1.56 as stated in the Sect. 2.3. The sampling was interrupted for a minute to avoid a turn.

Deleted: Page Break

¶

¶

Figure 9. Bypass test

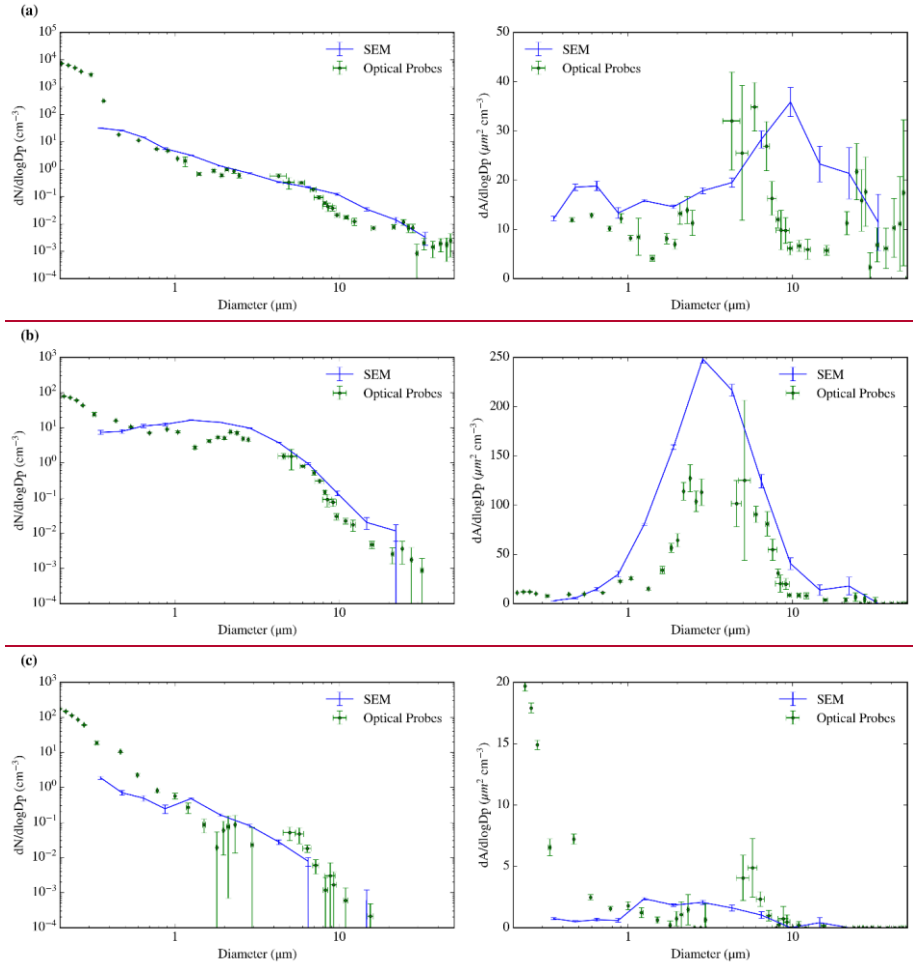

Figure 9. SEM obtained size distribution compared with PCASP-CDP online size distribution for three different sampling periods in three different aerosol environments. Close to London, on the 2017/07/19 (flight C024) from 15:20 to 15:51 UTC, sampling 953 L (a), south of Iceland on the 2017/10/02 (flight C059) from 16:24 to 16:40 UTC, sampling 432 L at an altitude of about 320 m, (b) and in north Alaska on the 2018/03/20 (flight C090) from 20:15 to 20:37, sampling 724 L (c). All the sampling was done in the upper line with the bypass open. The flow rates through the filter holders are 30.9, 30.5 and 42.0 L min^{-1} respectively. The optical probes are the PCASP-CDP, using the closest calibration to the sampling date and a refractive index of 1.56 as stated in Sect. 2.3.

Deleted: ¶
¶

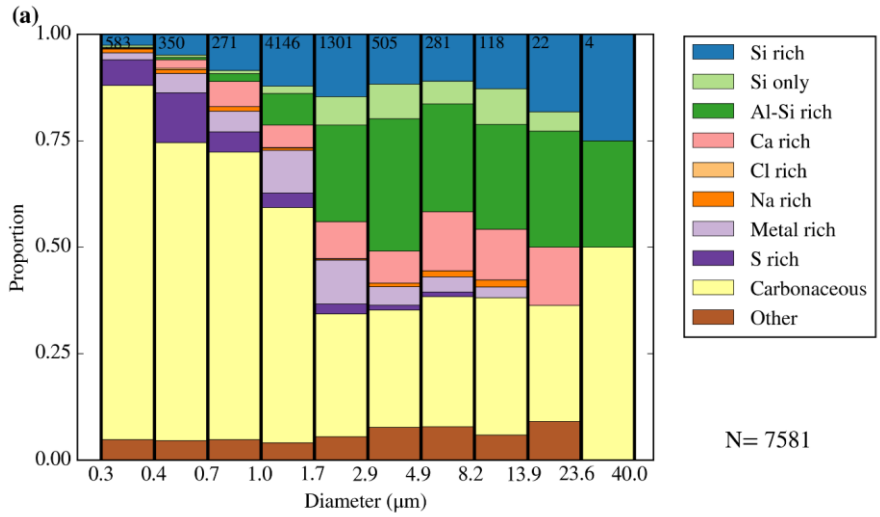
(a)
1.00
0.75
0.50
0.25
0.00
Proportion
583
350
271
4146
1301
505
281
118
22
4
0.3
0.4
0.7
1.0
1.7
2.9
4.9
8.2
13.9
23.6
40.0
Diameter (μm)
Si rich
Si only
Al-Si rich
Ca rich
Cl rich
Na rich
Metal rich
S rich
Carbonaceous
Other
N= 7581

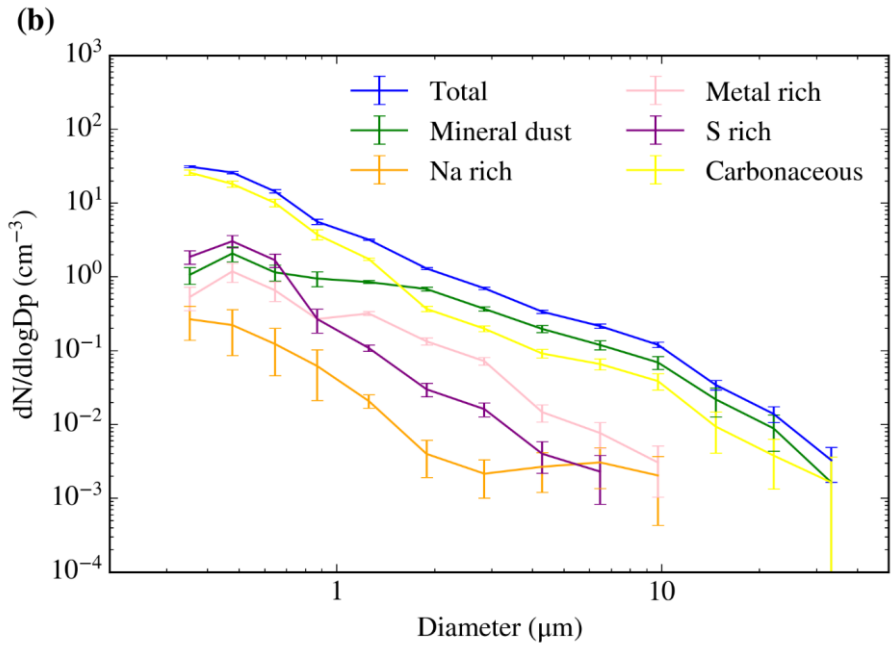
(b)
Total
Mineral dust
Na rich
Metal rich
S rich
Carbonaceous
dN/dlogDp (cm^{-3})
Diameter (μm)

1427

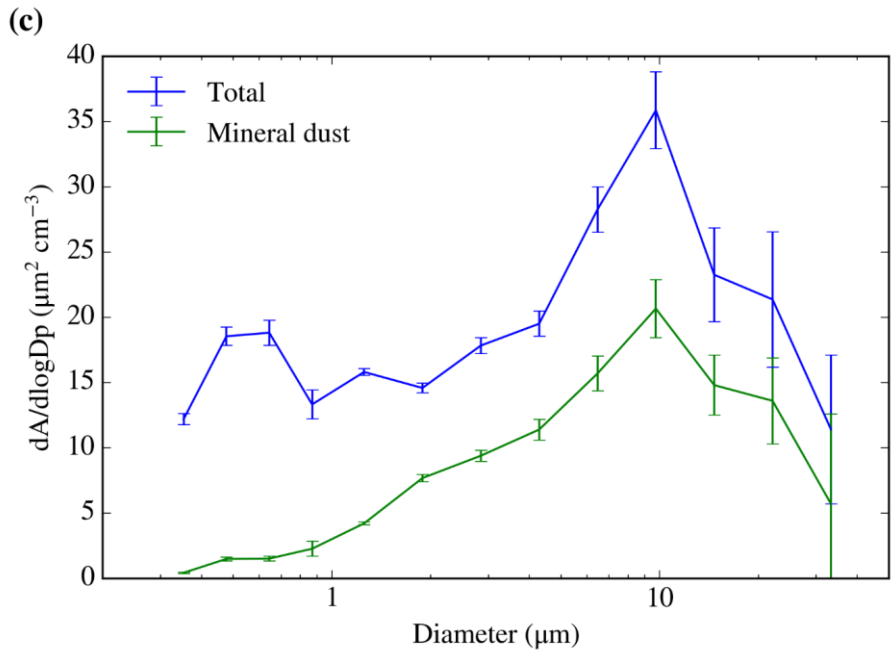
(c)
Total
Mineral dust
dA/dlogDp (μm^2 cm^{-3})
Diameter (μm)

1428

Figure 10. Size-segregated compositional and morphological analysis of a sample collected close to London (S.E. England) on the 2017/07/19 from 15:20 to 15:52 UTC by the lower line with the bypass open, sampling a total of 953L at 350 m altitude. (a) Fraction of particles corresponding to each compositional category (described in the Appendix B) for each size. The number of particles per bin can be seen in the top of the figure. (b) Number size distribution for each composition. Cl rich particles were not included since only two particles in this category were found. The errors have been calculated from the Poisson counting statistics (applying it to both the size distribution and the compositional measurements). (c) Surface area of both all the detected aerosol particles and the ones whose composition was consistent with mineral dust. Errors have been calculated in the same way as before. By integrating the green curve in the figure (c) we obtained the total surface area of mineral dust in the sample (19.1 $\mu m^2\ cm^{-3}$).

Deleted: xxx

Deleted: ¶

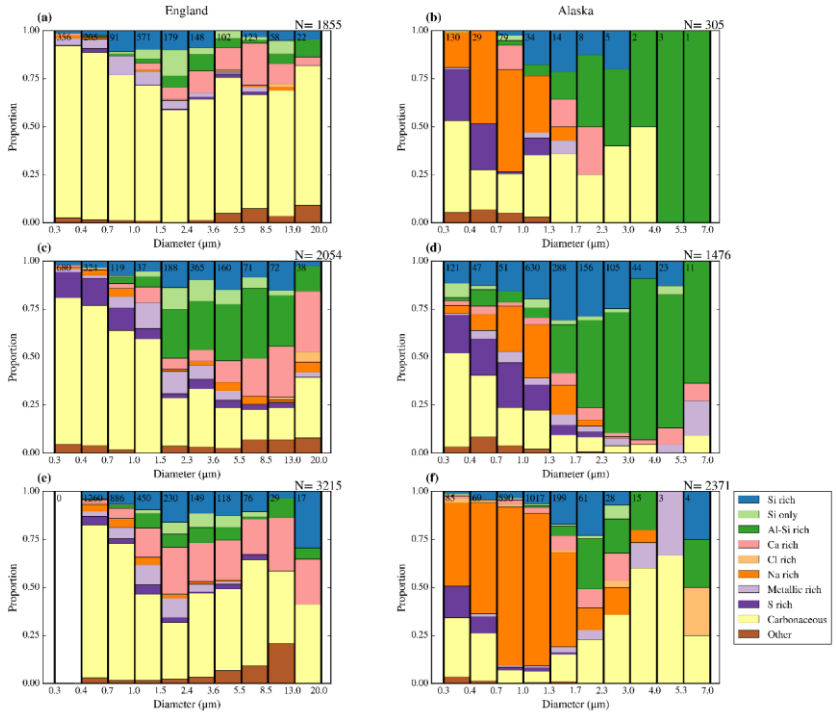

Figure 11. Six examples of the size resolved composition of aerosol sampled from the BAe-146 aircraft above South England (a, c and e) and North Alaska (b, d and f). All the samples were taken with the bypass open. The dates and sampling times (in UTC) are: (a) 2017/07/17 (flight C022) from 9:29 to 9:41, sampling a total of 182 L at an altitude of about 240 m, (b) 2018/03/18 (flight C089) from 19:28 to 19:48, sampling a total of 404 L at an altitude of about 600 m, (c) 2017/07/19 (flight C024) from 15:20 to 15:52, sampling a total of 256 L at an altitude of about 350 m (this sample was taken on the same that as the one shown in Fig. 10), (d) 2018/03/20 (flight C090) from 20:15 to 20:37, sampling a total of 724 L at an altitude of about 520 m, (e) 2017/07/20 (flight C025) from 12:51 to 13:09, sampling a total of 425 L, (f) 2018/03/21 (flight C091) from 18:27 to 18:56, sampling a total of 1187 L at an altitude of about 120 m at an altitude of about 940 m.

Deleted: 6

Deleted: at

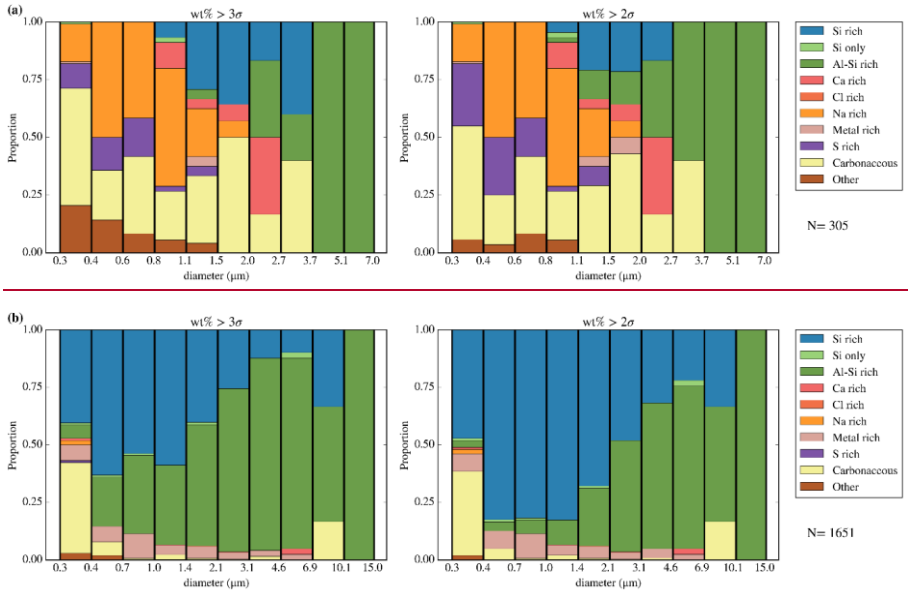

Figure C1. Size-segregated composition of two aerosol samples for different element detection confidence levels. The samples are 2018/03/18 from 19:28 to 19:48 UTC in north Alaska (a) and 2017/10/02 from 16:24 to 16:40 UTC in Iceland (b). The two samples are very different since the first sample presented a very low aerosol loading and it is dominated by Na rich particles, Carbonaceous and mineral origin aerosol (Si rich, Si only, Al-Si rich) with significant contributions of S rich particles whereas the second sample presented a high aerosol loading and it was mainly dominated by mineral origin aerosol. The different in the confidence mainly affected the Si and Al-Si rich particles as well as the S rich particles in the sample (a), whereas it only affected the Si and Al-Si rich particles in the sample (b).